



Rupert Lenzenweger, BSc

UV-vis spectroscopy for NO/NO₂ concentration measurements in exhaust gas

MASTER'S THESIS

to achieve the university degree of

Diplom-Ingenieur

Master's degree programme: Technical Physics

submitted to

Graz University of Technology

Supervisor

Ao.Univ.-Prof. Dipl.-Ing. Dr.techn. Roland Resel

Institute of Solid State Physics

Co-Supervisor

Univ.-Prof. Mag.rer.nat. Dr.rer.nat. Alexander Bergmann

Institute of Electronic Sensor Systems

ABSTRACT

Recently exhaust gas and nitrogen oxides got a lot of media attention. Chemiluminescence measurements are not well suited for mobile measurements and new methods are necessary. In this work two methods for qualitative and quantitative mobile nitrogen oxide detection, absorption and fluorescence spectroscopy, are investigated. Besides the general possibility to measure nitric oxide, the problems which occur when using these methods for exhaust gas measurements are discussed. The main problem is the huge cross-correlations from other occurring gases such as sulphur dioxide, ammonia or aromatic hydrocarbons, which are developed in a combustion engine besides the main components nitrogen and carbon dioxide.

Measurements were performed with different mixtures of nitrogen, NO, NO₂ and synthetic air. Due to the quenching effect of carbon dioxide and oxygen and the resulting necessary preparation of the gas, dilution with N₂, fluorescence measurements are restricted to a stationary measurement but with a high sensitivity and selectivity. Therefore this method could become a potential alternative to the common chemiluminescence measurements. Promising results were achieved using the absorption method in relation to the desired resolution. When using absorption spectroscopy the separation of the cross correlations is a demanding, but tests with NO₂ as background gas led to good results, the same as for simulations due to the distinctive absorption peaks of NO.

Vor kurzem erst waren Abgas und speziell Stickoxide ein großes Thema in den Medien. Chemilumineszenz Messungen sind für die mobile Messung von Stickoxiden nicht geeignet, neue, mobile Messmethoden sind nötig. In dieser Arbeit werden zwei Methoden für die qualitative und quantitative mobile Stickoxid Detektion, Absorption und Fluoreszenz Spektroskopie, untersucht. Neben der generellen Möglichkeit der Stickstoffmonoxid Detektion werden Probleme behandelt, die sich für die gewählten Messmethoden für Abgase ergibt. Das größte Problem ist dabei die große Überlagerung von anderen auftretenden Gasen wie Schwefeldioxid, Ammoniak und aromatischen Kohlenwasserstoffen, welche bei Verbrennungsvorgängen in einem Motor neben den beiden Hauptkomponenten Stickstoff und Kohlendioxid entstehen.

Messungen mit verschiedenen Mischungen von Stickstoff, NO, NO₂ und synthetischer Luft wurden durchgeführt. Wegen des Quenching Effekts von Kohlendioxid und Sauerstoff und die daraus resultierende notwendige Gasaufbereitung, eine Verdünnung mit N₂, sind Fluoreszenzmessungen auf eine stationäre Messung, welche aber eine hohe Sensitivität und Selektivität hat, beschränkt. Eine solche Messung könnte eine mögliche Alternative für die übliche Chemilumineszenz Messung werden. Vielversprechende Resultate in Bezug auf die angestrebte Auflösung sind bei der Absorptionsmethode erreicht worden. Dabei ist die Trennung von Überlagerungen das größte Problem, jedoch haben Tests mit NO₂ als Hintergrundgas gute Resultate, ebenso wie Simulationen, gezeigt.

ACKNOWLEDGEMENTS

First of all I would like to thank my supervisor Gerald Auböck and his team at CTR, particularly Jozef Pulko and Cristina Consani, for the opportunity to work in their group and their help during my work.

Also, I want to thank Alexander Bergmann and his team for his supervision and help during the thesis and for a vast number of discussions which helped promote my thesis. Further, I want to thank Roland Resel for his supervision, having an eye on the formal guidelines and the help with the organisation of this thesis.

I also want to thank my family for their support through out my studies and thesis. Particularly I want to thank my girlfriend, Marie-Christine, who encouraged me through tough and exhausting times in my studies.

This work was funded by the Austrian government within the ASSIC Comet program.

AFFIDAVIT

I declare that I have authored this thesis independently, that I have not used other than the declared sources/resources, and that I have explicitly indicated all material which has been quoted either literally or by content from the sources used. The text document uploaded to TUGRAZonline is identical to the present master's thesis.

Date

Signature

EIDESSTATTLICHE ERKLÄRUNG

Ich erkläre an Eides statt, dass ich die vorliegende Arbeit selbstständig verfasst, andere als die angegebenen Quellen/Hilfsmittel nicht benutzt, und die den benutzten Quellen wörtlich und inhaltlich entnommenen Stellen als solche kenntlich gemacht habe. Das in TUGRAZonline hochgeladene Textdokument ist mit der vorliegenden Masterarbeit identisch.

Datum

Unterschrift

TABLE OF CONTENTS

	Page
List of Tables	vii
List of Figures	viii
1 Introduction	1
1.1 Motivation	1
1.1.1 Current Situation	1
1.1.2 Advantages of UV-Spectroscopy	2
2 Fundamentals	3
2.1 Exhaust Gas	3
2.1.1 Euro 6 regulation	3
2.2 Gas Measurements: An Overview	5
2.3 Electronic Absorption	5
2.3.1 Lambert-Beer Law	6
2.3.2 NO Absorption	7
2.3.3 NO ₂ Absorption	8
2.3.4 Other expected gases	9
2.4 Fluorescence	12
2.4.1 Kasha's rule	12
2.4.2 Fluorescence Quenching	12
2.4.3 NO fluorescence	16
2.4.4 Fluorescence of other expected gases	18
2.5 Fabry-Pérot Etalon	20
2.5.1 Etalon comparison	22
3 Experimental	25
3.1 Absorption spectroscopy	25
3.1.1 Concept	25
3.1.2 Experimental setup	26

3.1.3	Custom made absorption cell	27
3.2	Fluorescence spectroscopy	30
4	Results and Discussion	34
4.1	Mass flow controller	34
4.2	Fluorescence measurements	34
4.2.1	Dark measurements	35
4.2.2	Measurements with synthetic air	35
4.2.3	Nitric oxide and nitrogen	36
4.2.4	Nitric oxide and synthetic air	39
4.2.5	Nitric dioxide measurements	42
4.2.6	Nitric oxide and nitric dioxide ratios	43
4.2.7	Discussion of fluorescence measurements	44
4.3	Absorption measurements	45
4.3.1	Influence of the Xe-Flash lamp on the calibration gases	45
4.3.2	Experimental approach and data analysis	48
4.3.3	Detection limit	49
4.3.4	Manual controlled etalon measurements	51
4.3.5	Discussion	54
5	Conclusion and Comparison	56
6	Appendix	58
6.1	Pulse energy	58
6.2	Used parts and devices	60
	Bibliography	61

LIST OF TABLES

TABLE	Page
2.1 Euro 6 regulations for the emission of exhaust gas for petrol engines and diesel engines with values for carbon monoxide (CO), aromatic hydrocarbons (HC) and nitrogen oxides.	4
2.2 Data from table 2.1 in ppm	4
2.3 Concentrations of hydrocarbons in exhaust gas [9], [33]	10
2.4 Calculated lifetimes of the different vibrational levels of the γ -band [3]	16
2.5 Quenching rate coefficients for the $A^2\Sigma$ state. The excitation was done with a 226 nm laser and the rates were investigated for the transition $A^2\Sigma v' = 0 \rightarrow X^2\Pi v'' = 3$, in units of $[10^{-10} \text{ cm}^3 \text{ molecule}^{-1} \text{ s}^{-1}]$ [8]	18
4.1 Number of measurements for the NO/N ₂ investigation, concentrations given for NO.	36
4.2 Number of measurements for the NO/synthetic air investigation, concentrations given for NO.	39
4.3 Number of measurements for the NO-NO ₂ measurements	43
6.1 Used parts in the setups, parts used in both setups are listed first.	60

LIST OF FIGURES

FIGURE	Page
2.1 Driving Cycles	4
2.2 Jablonski diagram	5
2.3 Schematic photodissociation	6
2.4 NO absorption cross section	7
2.5 NO energy band diagram	8
2.6 NO-NO ₂ concentration dependency	8
2.7 NO ₂ absorption cross section	9
2.8 Absorption cross section of selected aromatic hydrocarbons	11
2.9 NH ₃ absorption cross section	11
2.10 Schematic of Kasha's rule	13
2.11 Stern-Volmer plot	14
2.12 Temperature dependency of collisional and static quenching	14
2.13 Fluorescence spectrum of NO	17
2.14 Concentration dependency of NO fluorescence	17
2.15 Pressure dependency of NO self quenching	18
2.16 SO ₂ fluorescence	19
2.17 Naphtalene fluorescence	20
2.18 Temperature dependency of naphthalene fluorescence	20
2.19 Toluene fluorescence	21
2.20 Etalon interference	21
2.21 Schematic etalon	22
2.22 NO absorption cross section and etalon transmission comparison	23
2.23 Transmission etalon 5	24
2.24 Transmission etalon F	24
3.1 Xe-flash lamp spectrum	27
3.2 Absorption setup schematic	28
3.3 Absorption setup	29
3.4 Fluorescence setup schematic	31

3.5	Fluorescence setup	32
3.6	Filter flash lamp lines	33
4.1	PMT dark signal	35
4.2	Background signal fluorescence	36
4.3	NO-N ₂ fluorescence	37
4.4	NO fluorescence concentration dependency	38
4.5	NO-synthetic air fluorescence	40
4.6	NO-N ₂ fluorescence	40
4.7	NO-synthetic air fluorescence dependency	41
4.8	NO ₂ fluorescence signal	43
4.9	NO-NO ₂ fluorescence	44
4.10	NO-NO ₂ fluorescence, more detail	44
4.11	NO, NO ₂ spectra with Xe-flash lamp exposure	47
4.12	NO and NO ₂ spectra after Xe-flash lamp exposure	47
4.13	NO ₂ concentration behaviour with flash lamp over time	48
4.14	Detection limit bread board setup	49
4.15	Detection limit absorption cell	50
4.16	Signal to NO Concentration	50
4.17	NO absorption signal etalon angle dependency	52
4.18	NO ₂ absorption signal etalon angle dependency	52
4.19	NO absorption signal simulation comparison	54
4.20	NO absorption signal with optimized etalon	54
6.1	Spectral distribution of L9455-01 flash lamp	58
6.2	Waveform difference	59

INTRODUCTION

1.1 Motivation

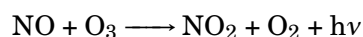
Acid rain, cancer and oedema are the worst damages to humans and nature caused by nitric oxides. NO and NO₂ are mainly produced by combustion-engines and the use of fossil fuels. In the year 2015 the nitric oxides were big in the media due to the exhaust scandal of VW. They were determining the inspection on the dynamometer with software and setting the engine in a special mode to reduce the emission of nitric oxides. The downside of this mode is less fuel economy and power. As the impact of these gases are enormous there is a lot of effort of governments to reduce the emission with always stronger regulations. As these regulations are not worth anything without a working control mechanism measurement methods are needed. As the current ones can be easily detected by engineers through software systems and avoided, it is necessary to develop new possibilities to get reliable results.

1.1.1 Current Situation

Not only the emission is strongly regulated also the measurement methods of exhaust gas are strongly controlled to get more or less comparable measurements. This means scientists are limited to certain effects. Due to this strong regulation only three measurement methods are possible to get a legal safe result.

- **Chemiluminescence**

Currently chemiluminescence is the used method to measure NO in the exhaust gas. This method uses ozone to transform the exhaust NO to an excited NO₂.



The relaxation of the NO₂ molecule leads to an emission of a photon. This photon can be

easily detected with a photomultiplier. The detected signal is proportional to the NO concentration. This measurement method can only detect NO and therefore other NO_x molecules have to be converted to NO. This is done with a reaction chamber. To get the ratio of NO_x to NO measurements with and without reaction chamber are necessary. Although this method is used today and it is usable for mobile measurements the usage as a mobile measurement system in cars is not safe due to the high toxicity of ozone. The safety limit for ozone is at 85 ppb and due to this restrictions the chemiluminescence method is limited to stationary measurement were the vehicles are operated on a dynamometer.

- **Infrared spectroscopy**

Infrared spectroscopy method uses wavelengths greater than 780 nm to determine the gas concentration. Problem for the NO_x measurements is the weak interaction of NO and NO₂ in this region and the huge cross-correlation with other exhaust gases like H₂O and CO₂. As these gases make up nearly 30 percent of the exhaust gas (see section 2.1) is is not possible to measure reliably concentrations of NO and NO₂ in the range of a few ppm.

- **Non-dispersive UV-spectroscopy**

UV-spectroscopy method is similar to the Infrared spectroscopy only the used light is in a different range and no dispersive element can be used. This method uses UV light with wavelengths between 200 and 450 nm to determine gas concentrations. The measurement is possible since NO and NO₂ are strong absorbing in this wavelength area due to their molecular structure. In contrast to infrared spectroscopy where the measurement method is also limited because of the cross-correlations with other exhaust gases, cross-correlations are narrow and can be extracted (see section 2.3.4).

1.1.2 Advantages of UV-Spectroscopy

When measurements do not have to be in conformity with the law other measurements methods can be used. A quite common way are semiconductor sensors to measure gases and their concentration. In comparison to this measurement method UV-spectroscopy has advantages.

A permanent measurement is possible because there is no saturation effect which often occurs while using semiconductor sensors. Also there is no ageing effect on surfaces. The possibility of a simultaneous measurement of different gases with nearly the same setup is also favourable. In contrast to the semiconductor sensors the setup has to be a little bit larger but it can be build much smaller than a usual chemiluminescence setup and is therefore more mobile.

FUNDAMENTALS

2.1 Exhaust Gas

Exhaust gas of combustion engines consists to 71% of molecular nitrogen which is quite obvious since air, used for the combustion consists of nitrogen to about 78%. Nitrogen, carbon dioxide (14%) and water vapour (13%) make up 98% of the automotive exhaust [29]. The other two percent of gas are made up by carbon monoxide, nitride oxides and hydrocarbons. Some of these hydrocarbons are aromatic hydrocarbons, specially Toluene, Naphtalene and Benzene and are mostly emitted within the first kilometers of testing [9]. *"55—80% of the total aromatic hydrocarbon emissions occurred within the first kilometer of the NEDC"*

2.1.1 Euro 6 regulation

The emissions of the exhaust is regulated by the governments and the measurements are done with the "New European Driving Cycle" (NEDC) (cf. figure 2.1). The idea behind is to have a standardized test for cars on a dynamometer to get comparable values. The NEDC is used for emission tests following the Euro 6 b regulation. To have more realistic conditions the European parliament decided to switch the driving cycle from the NEDC to the "Worldwide Harmonized Light-Duty Vehicles Test Procedure" (WLTP), stated in the Euro 6 c regulation and starts at the 1st September 2017. A comparison between those two test is shown in figure 2.1.

Unfortunately these stationary tests can be easily detected by the software and the car can switch to a different engine setting to reduce the emission. A short overview is given about these regulations. The limits for the newest standard (Euro 6) are shown in table 2.1. This table also includes the particle mass and particle number regulations which are, however, not relevant for this thesis.

Table 2.1: Euro 6 regulations for the emission of exhaust gas for petrol engines and diesel engines with values for carbon monoxide (CO), aromatic hydrocarbons (HC) and nitrogen oxides.

Gas	Otto motor [mg/km]	Diesel engine [mg/km]
CO [mg/km]	1000	500
HC [mg/km]	100	
(HC + NO _x) [mg/km]		170
NO _x [mg/km]	60	80
Particle matter [mg/km]	4.5	4.5
Particle number [1/km]	6* 10 ¹² (Euro 6 b)	6*10 ¹¹
Particle number [1/km]	6* 10 ¹¹ (Euro 6 c)	6*10 ¹¹

The numbers in table 2.1 are cumulated mean values for the driving cycles. As those numbers are using the unit [mg/km] an approximation is needed to get values in ppm to have an idea what values are expected. The mean velocity for the NEDC is 34 km/h and for the WLTP it is 46.6 km/h. For the calculation a mean velocity of 40 km/h was estimated. The mean RPM is estimated with 3000 RPM. This leads to the ppm values in table 2.2.

Table 2.2: Data from table 2.1 in ppm

Gas	Otto motor [ppm]	Diesel engine [ppm]
CO	2541	1270
HC	91	
NO _x	107	142

These values are just an estimation for the real values. In the tests revealing the emission scandal the real values were by a factor of 5 to 20 higher than the US-regulations [28].

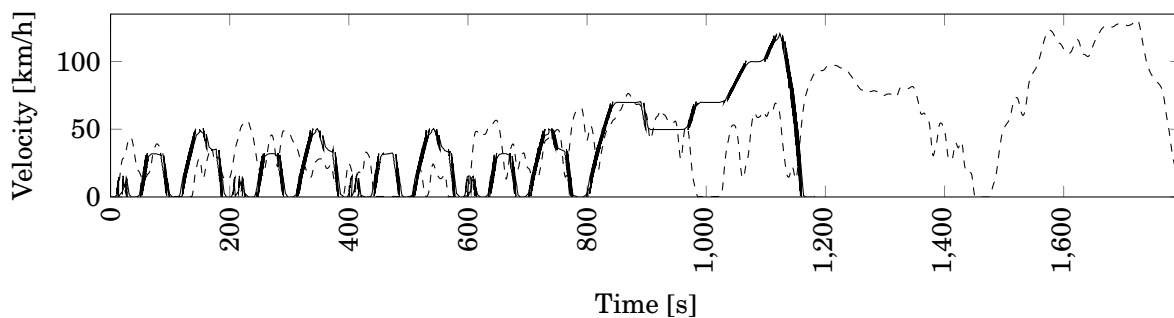


Figure 2.1: Velocity over time for the *New European Driving Cycle*, solid, and the *Worldwide Harmonized Light-Duty Vehicles Test Procedure*, dashed

2.2 Gas Measurements: An Overview

Although measurement methods for exhaust gas are restricted by law this section should give a short overview over the possible methods for gas measurements and their application. In the end all sensors give an electric signal as a function of the gas concentration. To generate this electric signal different chemical or physical effects are used, depending on the gas and the requirements on the sensor like the working environment, expected concentrations, selectivity, time resolution and others. Some sensors use semiconductors, oxide surfaces or polymers utilizing effects on their resistivity, others use surfaces which react with the gas and lead to a change of the temperature. Other used effects are the frequency change of an oscillating crystal, when molecules are adsorbed on the surface or a change in the thermal coefficient. In general gas sensors can be divided in two groups, mainly the **physical** and **chemical** sensors. [32] In the following sections only electronic absorption spectroscopy will be discussed due to the importance for the thesis. However usage of IR spectroscopy/FTIR spectroscopy is very important for gas measurements. Although it could be used to measure nitric oxide, an excellent and expensive FTIR spectrometer would be required.

2.3 Electronic Absorption

Basic knowledge about the effect and mechanism of absorption can be found in [1], chapter 2.6.

A short but detailed description is possible with a Jablonski diagrams, an example is shown in figure 2.2. The electronic states are depicted as S_0 , S_1 etc. This states are splitted in different vibrational energy levels, 0,1,2. If a photon is absorbed from the particle an electron from the ground-state (S_0) is lifted into an higher electron state according to the energy of the photon, which depends on the wavelength λ . (c.f equation 2.1)

$$(2.1) \quad E = \frac{hc}{\lambda}$$

c is the velocity of the light and h is the Plank-constant. Therefore a photon with a wavelength of 190 nm has an energy of 6.525 eV. As the energy depends inverse on the wavelength

electronic state transitions are only possible for stimulating photons with a small wavelength (< 1000 nm [6]). The absorption of photons with larger wavelengths result in vibration state

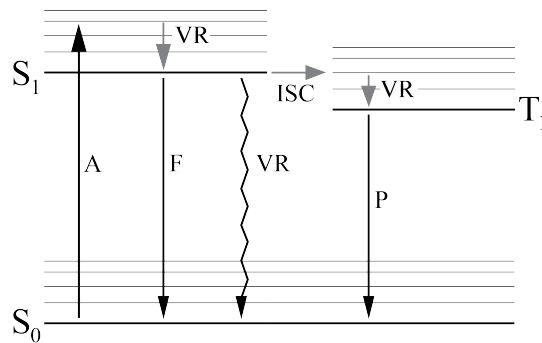


Figure 2.2: Jablonski diagram [10] S_0 is the ground state, S_1 the first excited state. The absorption process (A) excites the molecule in an excited state. It relaxes via vibrational relaxation (VR) to the lowest excited state. From this state different forms of relaxation are possible, namely the fluorescence (F), vibrational relaxation or an inter system crossing (ISC) to a triplet state (T_1) from where relaxation via phosphorescence is possible.

transitions ($1 \mu\text{m} < \lambda < 5 \mu\text{m}$ [6]) or rotational transitions ($30 \mu\text{m} < \lambda < 150 \mu\text{m}$ [6]). In general every electronic state transition is coupled to a vibrational and rotational transition (vibrational transitions are also coupled to a rotational transition). Another important principle for the absorption spectrum is the Franck-Condon principle. It gives the probability for the vibrational wave functions in the electrical states and therefore influences the height of the peaks in the absorption spectrum. For a detailed explanation of the principle please refer to [1].

As molecules tend to have the lowest possible energy it tends to emit the excess energy. To reduce the excess energy there are different possibilities. One of these processes is called fluorescence, c.f. section 2.4. Another process to reduce the energy is phosphorescence. Phosphorescence is described best when another state (often a triplet state) is inserted, a little bit lower in energy as the excited state. A transition takes place known as inter systems crossing to reduce its energy to the triplet state. This reduction is done via vibrational relaxation. From the triplet state the relaxation to the ground state is combined with the emission of a photon. In contrast to fluorescence the lifetime of the triplet state is much longer because triplet-singlet transitions are only allowed when a spin-orbit coupling occurs, typically τ is in the range of minutes to hours and therefore a afterglow is observed. Another possible process is the reduction to the ground state without emission of a photon. The excess energy is emitted as heat or as vibrational relaxation. If the energy of the photon is high enough it is possible that the excited electron will not occupy an unoccupied excited state in the atom. The atom is ionised. With a high enough photon energy it is also possible to dissociate a molecule. Therefore the photon excites the molecule on an anti bonding potential curve (cf. figure 2.3).

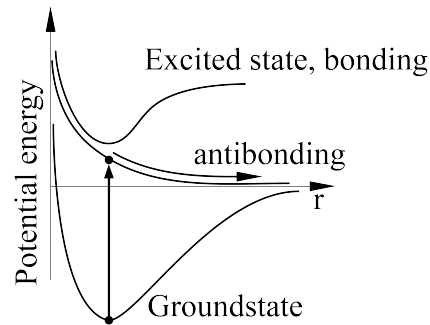


Figure 2.3: Energy diagram of photodissociation, an atom can be excited by absorption of a photon with the energy $\hbar\omega$ to a non-binding state [13]

2.3.1 Lambert-Beer Law

For the usage of absorption as a measurement principle a mathematical dependency is needed. The Lambert-Beer law (cf. equation 2.2) describes the relationship between the light intensity without absorbing material I_0 , the absorption coefficient $\epsilon(\lambda)$, the concentration of the absorbing substance c and the path length of light in the material d .

$$(2.2) \quad I = I_0 \cdot e^{-\epsilon cd}$$

The absorption coefficient in the formula is wavelength dependent and different for each substance. Due to the characteristic wavelength dependency it is possible to identify the substance. The law

is typically used in chemistry to determine the amount of substance fraction in liquid solutions but it is also suitable to calculate the concentration for gases or solids. [1]

2.3.2 NO Absorption

The absorption coefficient of nitric oxide is plotted in figure 2.4. The NO is for the most wavelengths transparent but has 4 characteristic peaks in the UV. With this peaks a pure NO sample is easily determined. Every peak is a different electron-vibrational transition. The 226.5 nm peak corresponds to the $X^2\Pi_r - > A^2\Sigma(0,0)$ transition. The transition $X^2\Pi_r - > A^2\Sigma(0,1)$ has a bigger energy gap and therefore must have a smaller wavelength. The peak at 214.4 nm corresponds to this transition [3]. These transitions ($X^2\Pi_r - > A^2\Sigma$) are referred to as γ -band. The two remaining peaks in the wavelength area this thesis takes a look at are also part of the γ -band, namely the transition $X^2\Pi_r - > A^2\Sigma(0,2)$ for the wavelength 204.8 nm and $X^2\Pi_r - > A^2\Sigma(0,3)$ for 195.5 nm. The association is done with the energy diagram of nitric oxide which is shown in figure 2.5 and the data from [31].

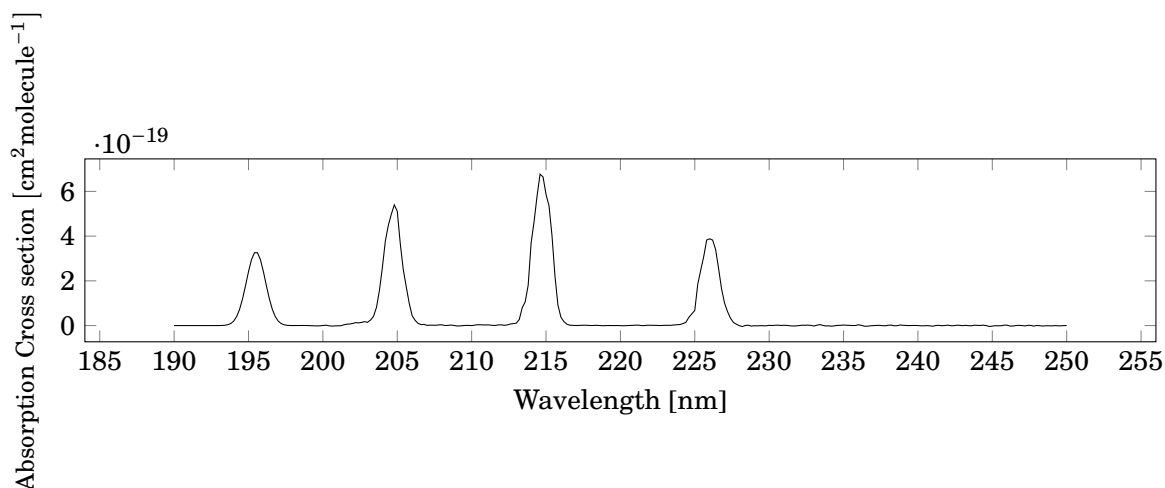
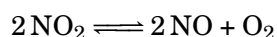


Figure 2.4: Absorption cross section of NO measured from Carinthian Tech Research AG (CTR AG), most up to date literature values at [12] are from 1963 and with low resolution. A comparison between the measured cross section and these values showed the peaks at the same wavelengths.

2.3.2.1 NO - NO₂ equilibrium

In presence of O₂ a conversion of NO to NO₂ is expected.



As shown in figure 2.6 at higher temperatures (> 200 °C) the equilibrium shifts to the right side of the reaction. This is due to the dissociation of NO₂. At lower temperatures a conversation of

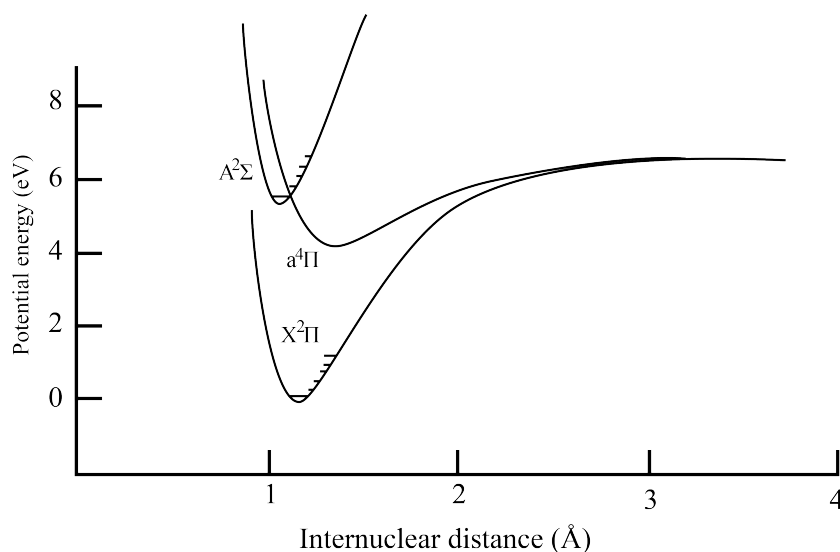


Figure 2.5: Energy band diagram for nitric oxide. For curves involved in the γ -band transitions some levels are indicated. [31] The $A^2\Sigma$ is well described by a harmonic oscillator in the lower range. This is the reason for the distinctive, nearly equally spaced absorption peaks.

NO to NO_2 should take place. This conversation is a very slow process since a 3 body collision is required to form NO_2 . In automotive catalysts the process is accelerated.

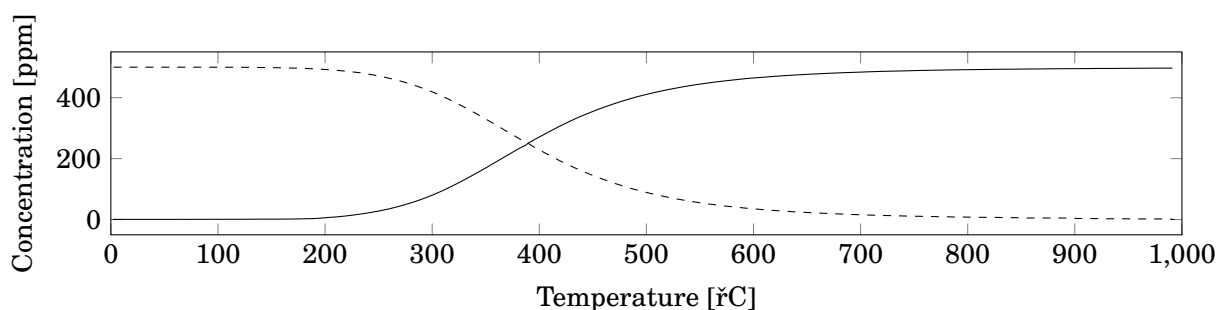


Figure 2.6: NO- NO_2 concentrations depending on the temperatures. NO: solid, NO_2 : dashed. [30]

2.3.3 NO_2 Absorption

Nitride dioxide does not have these characteristic sharp peaks since there are more possibilities for vibrational and rotational movements due to the third atom and therefore more possible absorption energies. Although there are more possibilities, the molecule has a more complex absorption spectrum as expected for a molecule with three atoms [5]. A possible explanation for this property is the coupling of the 2B_2 state with the high vibrational levels of the 2A_1 electronic ground state. Most of the absorption in the area of 250 nm to 900 nm are due to the $A^2B_2 \leftarrow X^2A_1$

transitions and gives the gas the brown-yellow colour at higher concentrations.

Due to the broad absorption spectrum of NO_2 up to 700 nm [12] and the sharp absorption peaks of NO it is easily possible to separate the contributions of the two molecules in the 200 to 250 nm region. The contribution of NO_2 absorption can be measured in a region (at around 400 to 450 nm) where no absorption from other gases is present. [5]

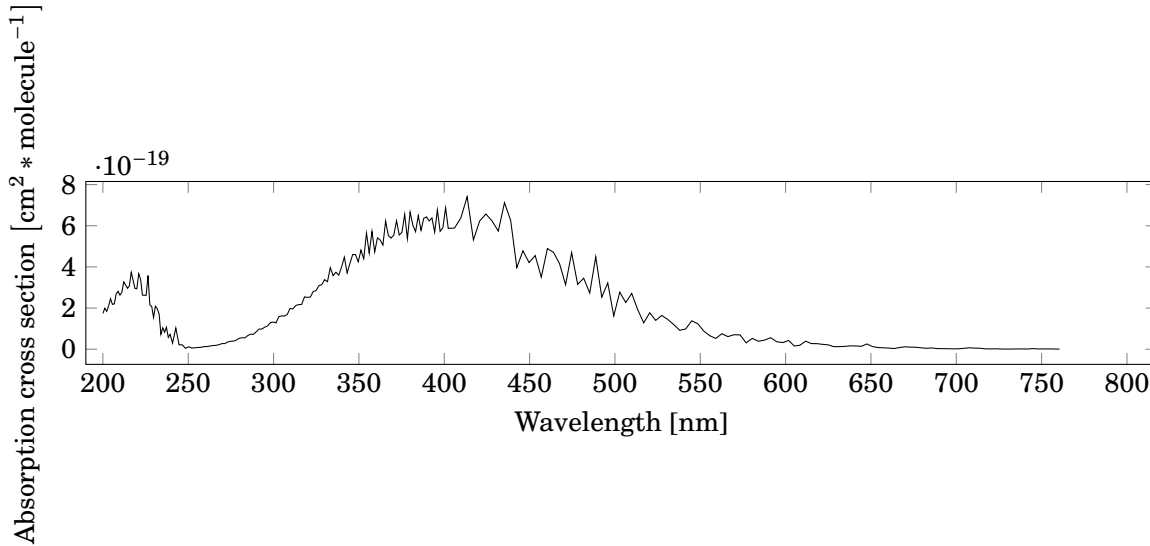
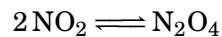


Figure 2.7: Absorption cross section of NO_2 [12]

NO_2 and its dimer N_2O_4

NO_2 has a common dimer which is N_2O_4 and both molecules exist in equilibrium.



The concentration of N_2O_4 reduces when the pressure is low and the temperature is high. At temperatures $> 135^\circ\text{C}$ mostly NO_2 is present. Because the system aims for a measurement of NO_2 in exhaust gas and this exhaust gas is quite hot (between 250°C when idling diesel engines and 1000°C for an otto motor at full load [7]) with a pressure in the area of 1 bar the dimer N_2O_4 is very small. This connotes nearly all molecules of the gas form NO_2 . Therefore a correction for the N_2O_4 contribution is not needed. [25]

2.3.4 Other expected gases

Since the main goal of the project is to measure the exhaust gas of auto mobiles it is important to consider possible cross correlations with other gases.

2.3.4.1 SO₂

The absorption spectra of different gases are shown in figure 2.8. As shown in this figure the absorption of SO₂ in the wavelength region of NO absorption is around the factor of 10 stronger. This connotes a high background signal and therefore an overlay over the NO signal. On the other hand modern fuels are desulphurised and therefore the expected concentration is more than a factor of 10 less than the ratio of nitrogen oxide. This means the cross correlation of SO₂ should reduce to a minimum and it should be possible to correct it with the methods used.

2.3.4.2 Aromatic hydrocarbons

In diesel or gasoline some aromatic hydrocarbons like toluene and naphthalene exist naturally. Aromatic hydrocarbons absorb strong in the region of nitric oxide as shown in figure 2.8. Comparing the absorption cross section with the one of NO shows an absorption of a factor of 100 and even 1000 stronger. Fortunately these molecules have a broad and flat absorption over the whole range. Expected concentration of aromatic hydrocarbons are in the range up to 24 ppm, see table 2.3. As stated in the section 2.1 and investigated in [9] these emissions mostly occur in the first kilometres of driving.

Table 2.3: Concentrations of hydrocarbons in exhaust gas [9], [33]

Aromatic hydrocarbon	with catalyst [ppm]	without catalyst [ppm]
Toluol	13	24
Benzene	4	7
Naphthalene	1	50

2.3.4.3 NH₃

The absorption spectrum of ammonia is shown in figure 2.9. The absorption of the biggest peaks is a factor of 100 bigger than for nitric oxide. However the absorption peaks with the longest wavelengths are at around 217 nm with an absorption cross section of $9 \cdot 10^{-19}$ and at 221 nm with $1.3 \cdot 10^{19}$. Those two have the same magnitude as the absorption of nitric oxide. Those peaks are not overlapping with those of nitric oxide and do not have the same spacing.

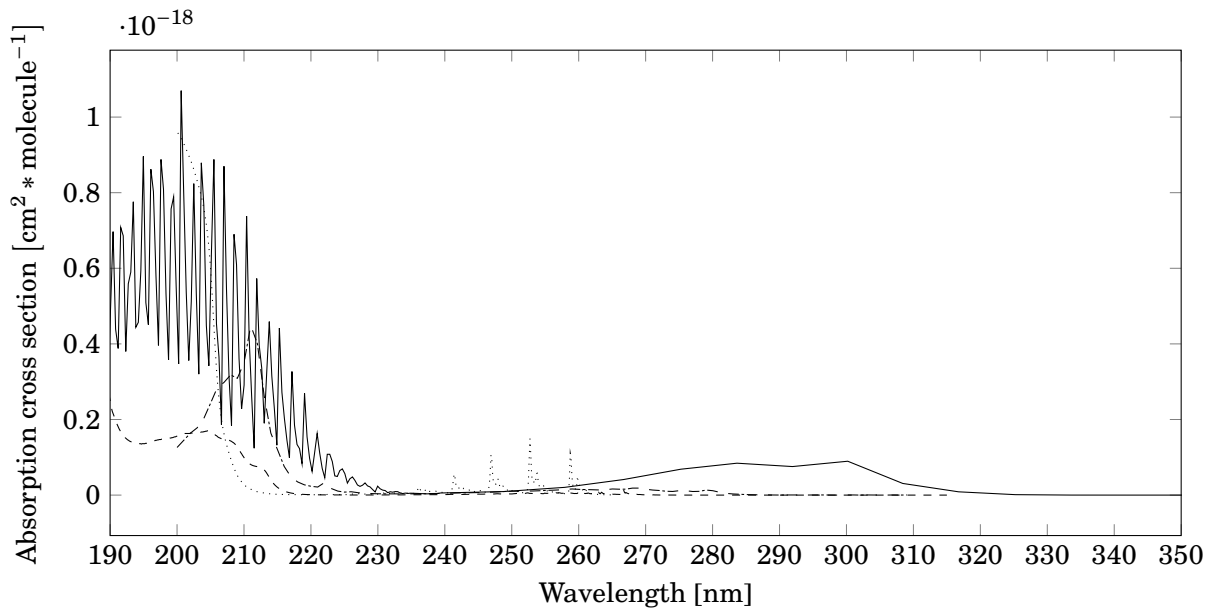


Figure 2.8: Absorption cross section of SO_2 (solid) and different aromatic hydrocarbons, namely Toluene (dashed, times 0.1), Benzene (dotted) and Naphthalene (dash pattern, times 0.01). The values for Toluene and Naphthalene are multiplied by the given factors to scale them for comparability. [12]

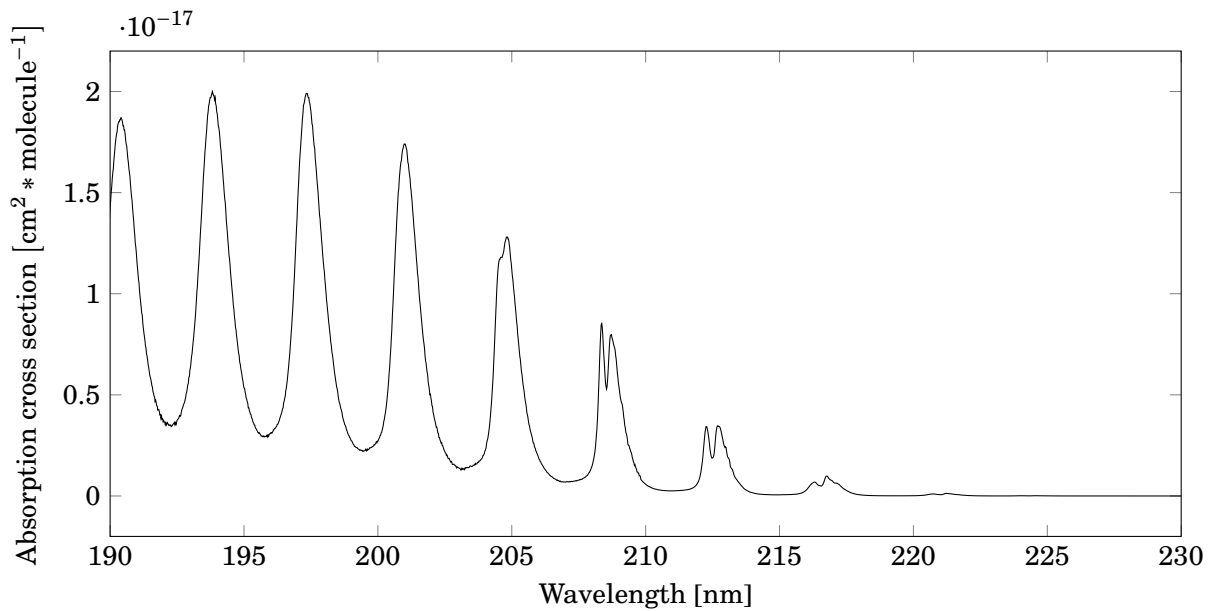


Figure 2.9: Absorption cross section of NH_3 . [12]

2.4 Fluorescence

Fluorescence is the reverse process of absorption. First a photon is absorbed and the atom or molecule is raised to a state of higher energy (cf. section 2.3, cf. figure 2.2). After a characteristic relaxation time (lifetime τ of the excited state) the particle relaxes to a lower state and emits a photon spontaneously with the energy according to the energy difference between the states. Therefore the highest possible energy of the fluorescence corresponds to the absorbed photon energy. The wavelength is reverse proportional to the energy (cf. equation 2.1). Due to the possibility of a relaxation to a state with higher energy than to the source state, e.g. the energy difference is smaller than the absorbed energy, and due to Kasha's rule (cf. subsection 2.4.1) the emission of photons with a higher wavelength is possible and common. Typically fluorescence lifetimes are in the range of 10^{-8} seconds [32]. In this spontaneous process the photon can be emitted in any direction in contrast to the stimulated emission where the direction of the emission is affected by the light which stimulates the emission. A factor to describe the probability of fluorescence is the quantum yield, which is the ratio between emitted photons and absorbed photons.

2.4.1 Kasha's rule

Excitation to an excited state which is not the lowest excited state leads to a short lifetime there. After this very short lifetime the molecule relaxes via vibrational relaxation to the lowest excited state. This process is typically faster than the lifetime of the lowest excited state. After the specific lifetime (c.f. NO lifetimes, table 2.4) in the lowest excited state the molecule relaxes to the ground state via emission of a photon according to the excess energy between those states. As this process of fluorescence is much slower than the relaxation to the lowest excited state the fluorescence wavelength is only expected to be equal or smaller than the longest absorption wavelength. In consequence the wavelength of the emission is only dependent on the energy difference between the lowest excited state and the ground states and is therefore independent on the excitation wavelength. This process is shown in figure 2.10.

2.4.2 Fluorescence Quenching

Fluorescence quenching is a reduction of fluorescence of a single molecule due to the presence of other molecules in the surrounding. It is possible to regain the fluorescence intensity when the quencher is removed. A quencher is not necessary a different atom or molecule as the fluorophore furthermore it is more likely to have a self-quenching effect where the fluorophore quenches itself. This effect occurs when the partial pressure, therefore the concentration of the fluorophore increases.

The most trivial quenching effects are reduced transmission of light like turbidity of the gas. But there are several principles which are more complex for example energy transfer, excited state

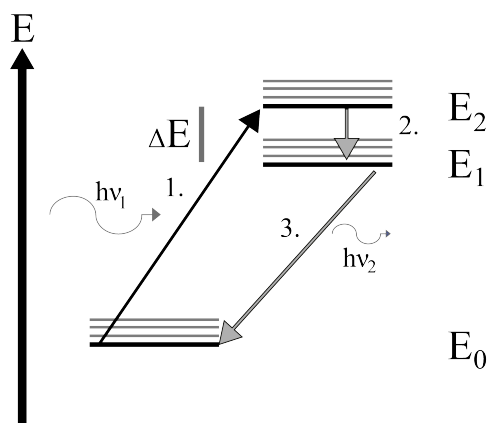


Figure 2.10: After the absorption of a photon with the energy $h\nu_1$ (1) the molecule is in an excited state E_1 and will relax via vibrational relaxation to the lowest excited state possible E_2 (2) from where the fluorescence process (3), where a photon with the energy $h\nu_2$ is emitted, takes place. [20]

reactions, coordination complex formation or collision quenching. For the more complex effects contact between the fluorophore and the quencher is necessary. The transport of the quencher particle to the fluorophore is done by diffusion, so it is time depended. [15]

Stern-Volmer relationship The main equation to describe the behaviour of fluorophores and their quenchers is known as Stern-Volmer relationship, equation 2.3.

$$(2.3) \quad \frac{F_0}{F} = 1 + K_x[Q]$$

In this formula F_0 describes the initial fluorescence intensity without the presence of the quencher. The fluorescence intensity when the concentration of the quencher ($[Q]$) is present is described as F . K_x is the Stern-Volmer constant which is the slope in the Stern-Volmer plot, where $\frac{F_0}{F} - 1$ is plotted against the concentration of the quencher $[Q]$ (cf. figure 2.11). K_x is called K_S for static quenching and K_D for dynamic e.g. collisional quenching. Important for the use of the Stern-Volmer relationship is that the accessibility to the fluorophore molecules for the quencher is equal for all molecules and only one quenching effect (cf. Static quenching, Collisional quenching) affects the fluorophore.

Static quenching The effect of complex formation between a quencher and the fluorophore is known as static quenching. This can happen either with a fluorophore in the ground state and the complex does not get excited or the quencher and the excited fluorophore form an excited complex. This excited complex can return to the ground state without the emission of a photon, so without fluorescence. The excess energy is emitted through heat. The binding constant K_S (cf. equation 2.4) is the quotient of the concentration of the complex $[F - Q]$ and the non complexed

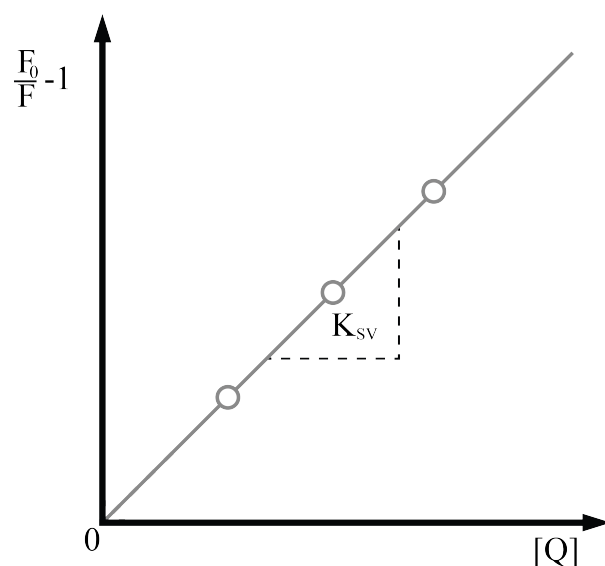


Figure 2.11: Stern Volmer plot. It is used to get the initial fluorescence without quenching. F_0 is the initial fluorescence intensity, F is the intensity with a certain concentration of the quencher $[Q]$. [22]

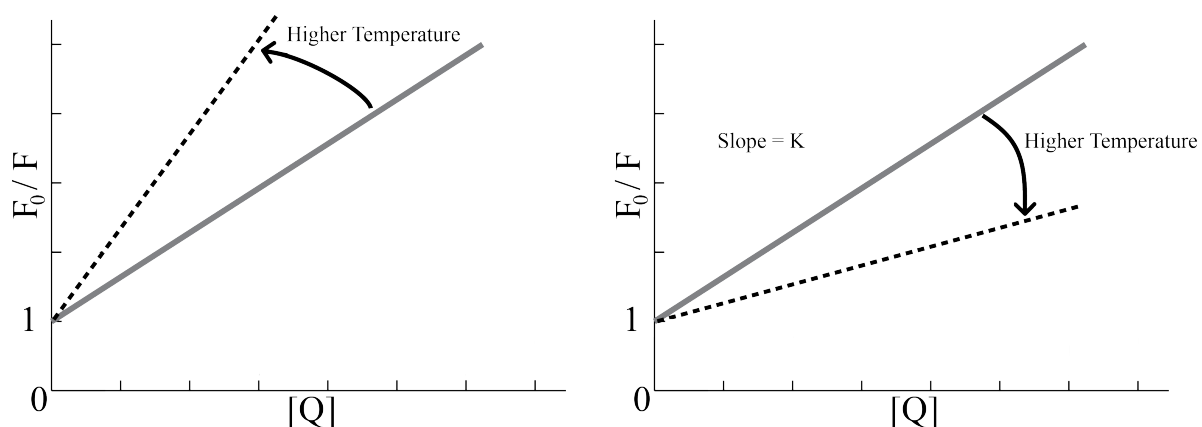


Figure 2.12: The temperature dependence of collisional (left) and static (right) quenching. As the temperature increases the molecules diffuse faster and the effect of collision quenching increases. On the right side a decrease of the quenching effect can be seen, when increasing the temperature. This is because of the low binding energies of formed complexes, K is the Stern-Volmer constant. [15]

fluorophore concentration $[F]$ and the concentration of the quencher $[Q]$.

$$(2.4) \quad K_S = \frac{[F - Q]}{[F][Q]}$$

For a non-fluorescent complex the formula transforms to equation 2.3, with F_0 as the initial fluorophore concentration, which indicates a linear dependency of the quencher concentration $[Q]$ with a factor of K_S .

Collisional quenching Collision quenching describes the effect when the quencher collides with the fluorophore and transfers the excited fluorophore to the electronic ground-state without the emission of a photon. The excess energy is discharged as heat.

In general *"any process that causes a decrease in intensity can be considered to be quenching."*
[15] The Stern-Volmer constant K_D can be calculated from

$$(2.5) \quad K_D = \tau_0 k_q$$

with τ_0 , the lifetime of the excited state of the fluorophore without the presence of the quencher and k_q is the bimolecular quenching constant. The bimolecular quenching constant is the product of the bimolecular coefficient k_0 and the quenching efficiency γ . The bimolecular coefficient describes the probability of a collision between the fluorophore particle and a quencher particle. The quenching efficiency gives the probability of a quenching effect, if the fluorophore and quencher collide. In other words the quenching efficiency is the probability that the quencher triggers a relaxation to the ground state of the fluorophore. The temperature dependency is shown in figure 2.12. When changing the temperature the type of quenching can be determined.

Resonance Energy Transfer - RET A different form of collisional quenching is the resonance energy transfer (RET). The energy of the fluorophore (in literature more general written as donor) transfers via RET to the quencher (acceptor). The acceptor can be fluorescent or not. An electron of the donor is excited through a photon (cf. section 2.3). This photon returns to the ground state without emission of a photon and an electron of the acceptor is lifted into an excited state. This electron transition occurs simultaneously and without physical contact of the two particles and is an effect of dipole-dipole interactions. The excited electron of the acceptor can now recombine with emission of a photon or recombine without emission and dissipate the excess energy as heat. In conclusion the main contrast of this effect to normal collisional quenching is that the distance between the two particles is larger than necessary for direct interactions.

Mechanism of quenching The last sections covered the possible forms of quenching but did not describe the mechanisms behind quenching. The mechanisms are:

- **Intersystem crossing** An excited singlet state can become an excited triplet state by a collision with a heavy particle. Triplet states have a much longer lifetime as singlet states hence their probability to be quenched by electron exchange or undergo a non-radiative decay is much bigger.
- **Electron exchange** The acceptor changes an unexcited electron in the ground state with the excited electron of the donor. This form of energy-exchange is similar to the mechanism of RET although the interaction distance is much smaller and the concentrations of the acceptor and donor has to be high. RET also occurs at lower concentrations.

Table 2.4: Calculated lifetimes of the different vibrational levels of the γ -band [3]

Level	Lifetime [sec]
2	$2.1 * 10^{-7}$
1	$2.1 * 10^{-7}$
0	$2.3 * 10^{-7}$

- **Photoinduced electron transfer** In this process a complex is formed between the donor and the acceptor. The donor is not necessarily the excited fluorophore, this depends on the oxidation potential of ground and excited states. The donor transfers an electron to the acceptor and two charged particles are formed.

To distinguish between collisional and static quenching the measurements of fluorescence lifetimes is possible. As the lifetimes of the uncomplexed fluorophore is still τ the factor $\frac{\tau_0}{\tau}$ equals 1. For the collision quenching the factor equals $\frac{F_0}{F}$. Another possibility to determine the type of quenching an absorption spectra can be measured. The collision quenching only affects the fluorescence of the fluorophore, the absorption spectra remains the same. In contrast when a complex is formed the absorption behaviour changes. As seen in the figure 2.12 another method to determine the main quenching process is to decrease or increase the temperature since both processes are temperature dependent. Collision quenching increases with rising temperature in contrast to a decrease of complex formation. The increase of collision quenching with increasing temperature is easy to understand since the average of the particle velocity increases at higher temperature and therefore the rate of collisions increases. The decrease of static quenching is because of the effect that weakly bond complexes will break up due to the increased temperature and therefore the quenching will decrease.

In most systems both effects are present which results in an not linear behaviour in the Stern-Volmer plot.

2.4.3 NO fluorescence

When doing UV-absorption with nitric oxide the γ -band transitions are investigated. When taking a look at the fluorescence spectrum these transitions are the ones observed. According to Schwarz and Okabe [26] the intensity of the fluorescence light is proportional to the incident light intensity and the concentration of NO up to 7 ppm. For concentrations higher than 7 ppm the effect of self-quenching must be considered in the analysis. A possible factor for a higher sensitivity are the different lifetimes of the different excited states, of a molecule and of different molecules. The resulting lifetimes of these transitions are in the range of 10^{-7} s (cf. table 2.4) and are at least one order of magnitude bigger than for usual fluorescence lifetimes. The quantum yield for the excitation at 214.9 and 204.8 nm is 1, which means they decay radiative to the ground state. [27]

They found in their research a nearly linear intensity dependency for values between 40 ppm and 250 ppm (c.f. figure 2.14). In the region below 1 ppm a linear dependency was shown.

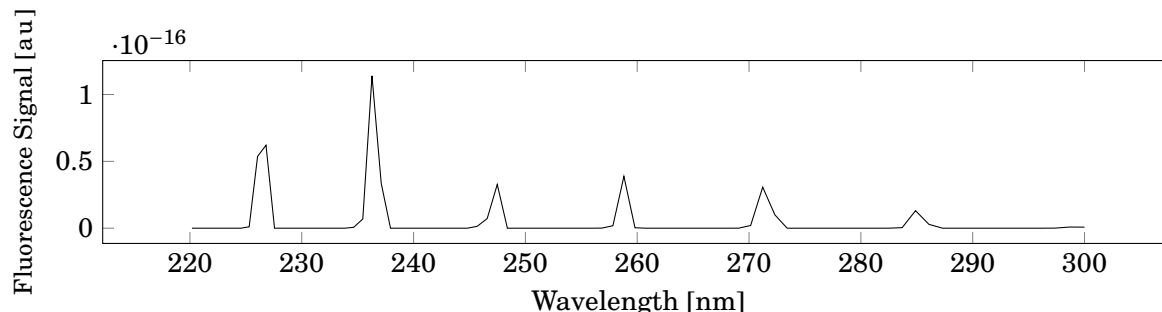


Figure 2.13: Expected fluorescence signal by an excitation wavelength of 226 nm [2]. As expected the wavelength of the fluorescence is shifted to lower energies, e.g. bigger wavelengths. Due to Kasha's rule it is not necessary to take other excitation wavelengths in account.

Quenching of NO fluorescence Self-quenching is for NO a function of pressure, the self-quenching half pressure is 0.96 mmHg, equal to 127.99 Pa (cf. figure 2.15 and [3]). Also the effect of absorption of fluorescence light adds a factor nearly as high as self-quenching. Investigations of this behaviour and afterwards comparing to known quencher showed, that CO_2 is about a factor of 2-3 more effective as self-quenching from the NO ground state for the $\text{A}^2\Sigma$. The pressure for half-quenching for CO_2 is 0.31 mmHg (in contrast to 0.91 mmHg for self-quenching) for 0.3 mmHg NO pressure, 100 mmHg total pressure [3]. They also evaluated the quenching rate of argon and molecular nitrogen. The half-quenching pressure of argon was determined at 1400 mmHg, 1.87×10^5 Pa. In some $\text{NO}+\text{CO}_2$ samples the added argon increased the intensity of the fluorescence by broadening the absorption lines, furthermore the collision-diameter for pressure broadening for the $\text{A}^2\Sigma$ state is 3.8 N_2 quenches the NO excited $\text{A}^2\Sigma$ state due to vibrational relaxation because the two molecules are very similar and therefore have similar vibrational levels. This vibrational energy transfer is not possible with Argon, but the overall quenching is nearly the same [4]. A similar result relating to the CO_2 quenching was found by Schwarz

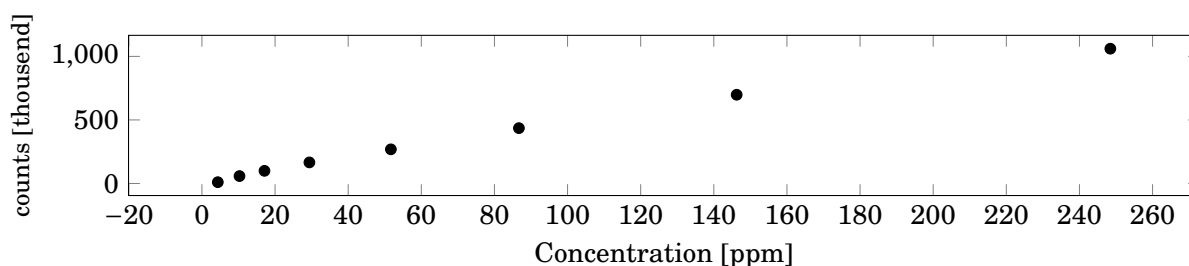


Figure 2.14: Nearly linear dependency of the concentration of NO to the fluorescence signal [21]

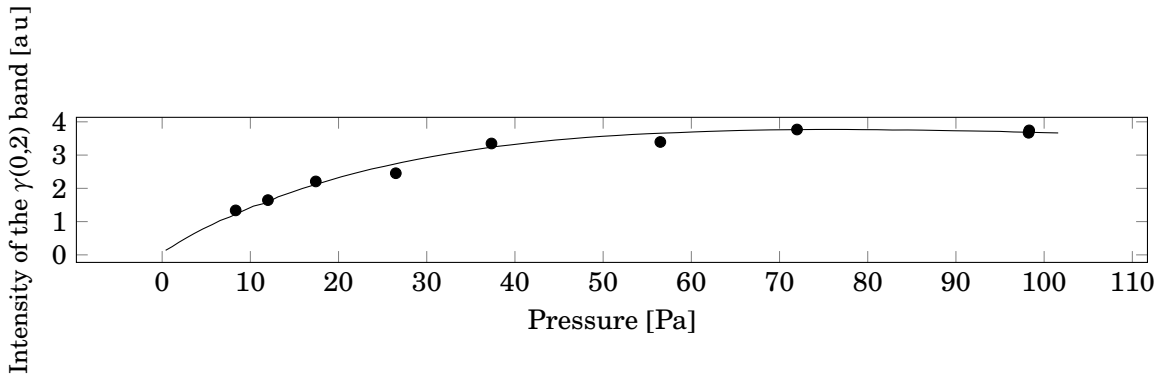


Figure 2.15: Pressure dependency of the self quenching effect of NO. [21]

and Okabe [26] which did measurements of the NO ratio in exhaust gas via fluorescence. They experimented with the most common exhaust gases. The quenching from H₂O and CO₂ is strong. A level of 5 % CO₂ quenches the signal of the NO fluorescence to a level of 0,03 % for an 1200 ppm sample [21]. They also investigated the influence of a dilution of the gas mixture with N₂ in the ratio of 1:100. This leads to an increase of the signal. This means the dilution has more effect on the quencher as on the fluorophore and is therefore a possibility to increase a quenched signal. Quenching rate coefficients for the A²Σ state of various gases are summarized in table 2.5. A further strong quenching gas is O₂. Melton [16] investigated the rate coefficients for quenching for $\nu = 0, 1$ and 3 and got $(1.6 \pm 0.2, 1.7 \pm 0.2$ and $1.6 \pm 0.2) 10^{-10} \text{ cm}^3 \text{ molecule}^{-1} \text{ s}^{-1}$.

Table 2.5: Quenching rate coefficients for the A²Σ state. The excitation was done with a 226 nm laser and the rates were investigated for the transition A²Σ ν' = 0 → X²Π ν'' = 3, in units of $[10^{-10} \text{ cm}^3 \text{ molecule}^{-1} \text{ s}^{-1}]$ [8]

NO	N ₂ O	H ₂ O	O ₂	CO ₂
2.67 ± 0.41	3.79 ± 0.49	7.8 ± 1.0	1.46 ± 0.25	4.30 ± 0.26

2.4.4 Fluorescence of other expected gases

Since fluorescence is the reverse process of absorption a closer look at the fluorescence properties of the discussed gases is necessary. An emission in the range of the nitric oxide fluorescence could be possible. Gases without an absorption spectrum in the range of the used light will not be excited.

2.4.4.1 NO₂ fluorescence

Increasing the pressure of NO₂ (or the carrier gas) the fluorescence shifts to the red due to partially relaxed molecules [19]. NO₂ fluorescence is heavily influenced by different processes of quenching e.g. multi step processes or strong collision quenching. [5]

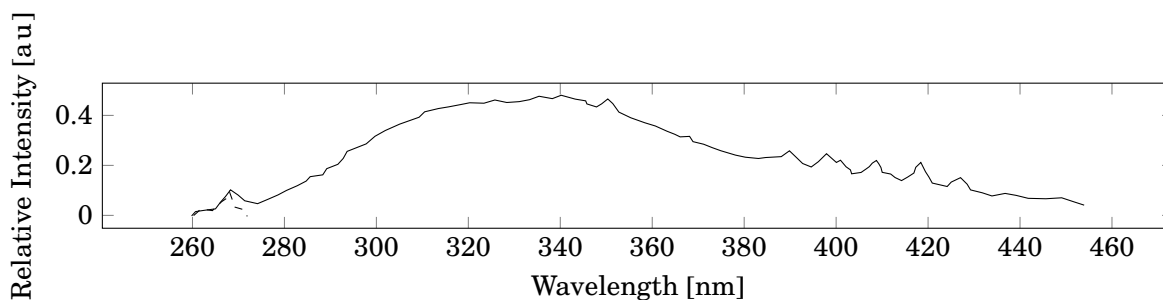


Figure 2.16: Fluorescence signal of SO_2 at a pressure of 666,6 Pa and an excitation wavelength of 265 nm. The dashed line is the scattered light [17].

2.4.4.2 SO_2

Fluorescence of SO_2 is a $A^1B_1 \rightarrow X^1A_1$ transition. The lifetime of this state decreases when the excitation energy gets bigger. SO_2 fluorescence shows efficient self-quenching when the pressure is increased. Collision between molecules quench very strong, nearly every collision leads to an electronical quenching to a lower state [17].

2.4.4.3 Aromatic hydrocarbons

As shown in the figure 2.8 aromatic hydrocarbons have a strong absorption in the UV. Therefore a fluorescence in the region of the NO fluorescence is possible.

Naphthalene Nearly all found literature use a 266 nm excitation wavelength. This wavelength corresponds to the $S_0 \rightarrow S_2$ transition. Molecules excited to the S_2 state change fast with a non-radiative vibrational relaxation to the lowest excited state S_1 . This behaviour is described by Kasha's rule. The fluorescence takes place from this state ($S_1 \rightarrow S_0$ transition). The spectrum is shown in the figure 2.17. The fluorescence is shifted to longer wavelengths. Orain, Baranger, Rossow and Grisch [23] found a strong quenching from O_2 for naphthalene fluorescence. Additionally they described a reduction of the fluorescence with increase in temperature (c.f. figure 2.18). The fluorescence quantum yield is a function of the wavelength and has a maximum for the shown wavelength (c.f. figure 2.17) at around 280 nm with 9 % [27].

Toluene Excitation at 248 nm and 260 nm leads to a fluorescence when using toluene gas. This fluorescence has a high quantum yield. Fluorescence of toluene is strongly quenched by oxygen which is used for measuring the pre combustion fuel-air mixture [24]. When using the excitation wavelength of 260 nm an exponential decrease with temperature of the quantum yield is investigated, using 248 nm as excitation wavelength the quantum yield decreases with a double exponential function of the temperature. Therefore they state a decrease of fluorescence with increasing temperature. [14]

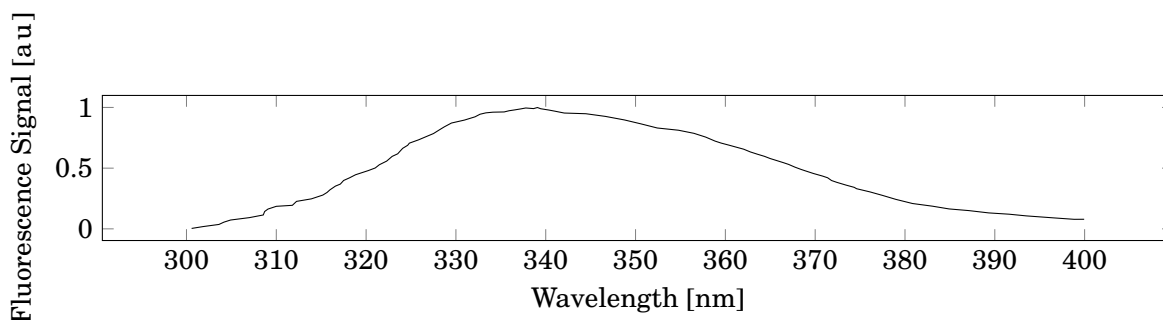


Figure 2.17: Fluorescence signal of naphthalene at a temperature of 350 K and an excitation wavelength of 266 nm. Although the excitation uses photons with energies in the UV range the fluorescence takes place in the UV and violet visible range (300 to 400 nm) as a consequence of Kasha's rule.[23]

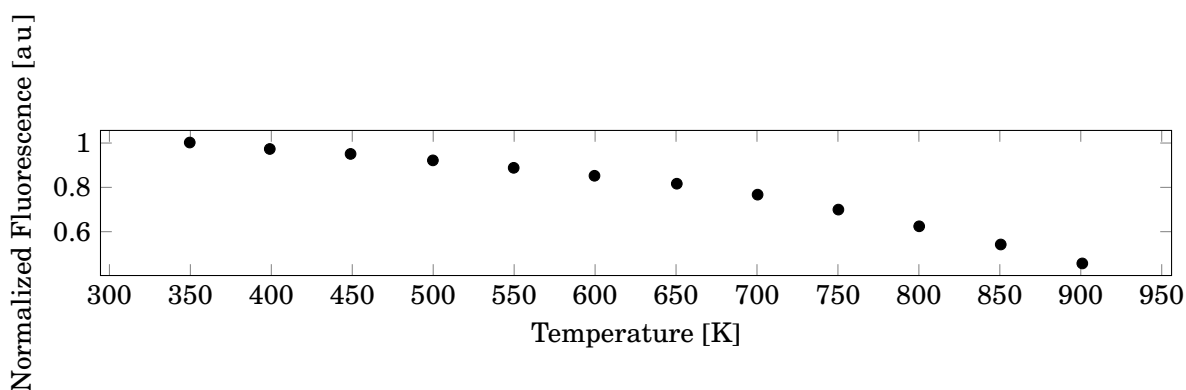


Figure 2.18: Decreasing fluorescence signal with increasing temperature of naphthalene. [23]

Benzene To measure fluorescence an excitation at 245 nm to 265 nm is necessary. Using an excitation wavelength shorter than 240 nm does not lead to any detectable fluorescence. In the possible wavelength range the quantum yield is low, for 259.1 the value is 0.12 [27].

2.5 Fabry-Pérot Etalon

The etalon is also known as Fabry-Pérot interferometer. A glass substrate is coated with two partly reflective films, mostly aluminium. The thickness of the layer is around 15 nm and the reflectance is 0.7. The thickness d of the glass substrate (cf. figure 2.21 and figure 2.20) defines the wavelengths which can pass the etalon due to constructive interference of a multiply reflected beam. The used etalon is a special designed to match the NO-absorption lines as best as possible (see subsection 2.3.2). Constructive interference is calculated with equation 2.6, z is the order of

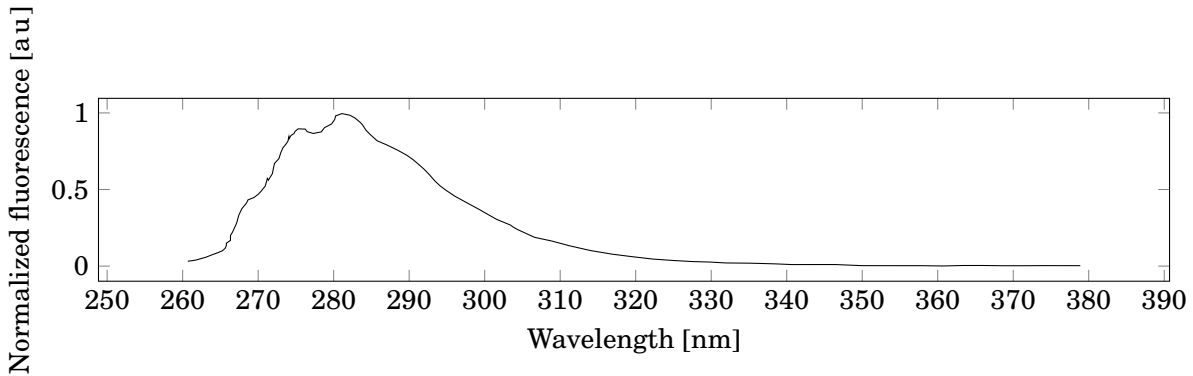


Figure 2.19: Fluorescence signal of 500 Pa toluene nitrogen at a total pressure of 10^5 Pa and 296 K. Excitation wavelength was 248 nm [14].

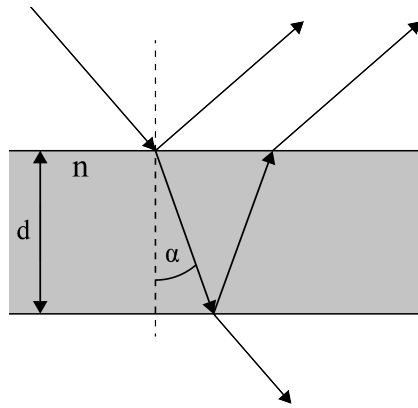


Figure 2.20: General description of the interference on the Fabry-Pérot etalon. Constructive interference is calculated with equation 2.6.

the interference.

$$(2.6) \quad z\lambda = 2d\cos(\alpha)$$

When the etalon is tilted by an angle β to the plain of incident of the beam the path-length of the light gets longer according to $x = \frac{d}{\cos(\beta)}$. This way it is possible to shift the transmission wavelength up to 8 nm before the frame of the etalon will interfere with the light. With this functionality it is possible to separate the contribution of NO from the underlying background absorption from other gases. This is due the distinctive absorption peaks, with them an increase in signal is detected when the transmission and absorption peaks overlap (c.f. section 3.1.1.1). A comparison between two possible angles, the absorption cross section of NO and NO₂ (as represent for cross correlations in the absorption range of NO) is in figure 2.22 shown. The transmission peaks do not match the absorption lines perfectly due to production tolerances. As in previous sections, basic knowledge can be found in [1], chapter 3.

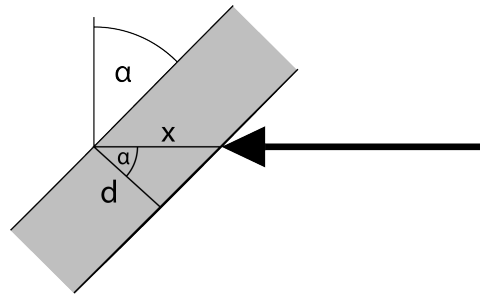
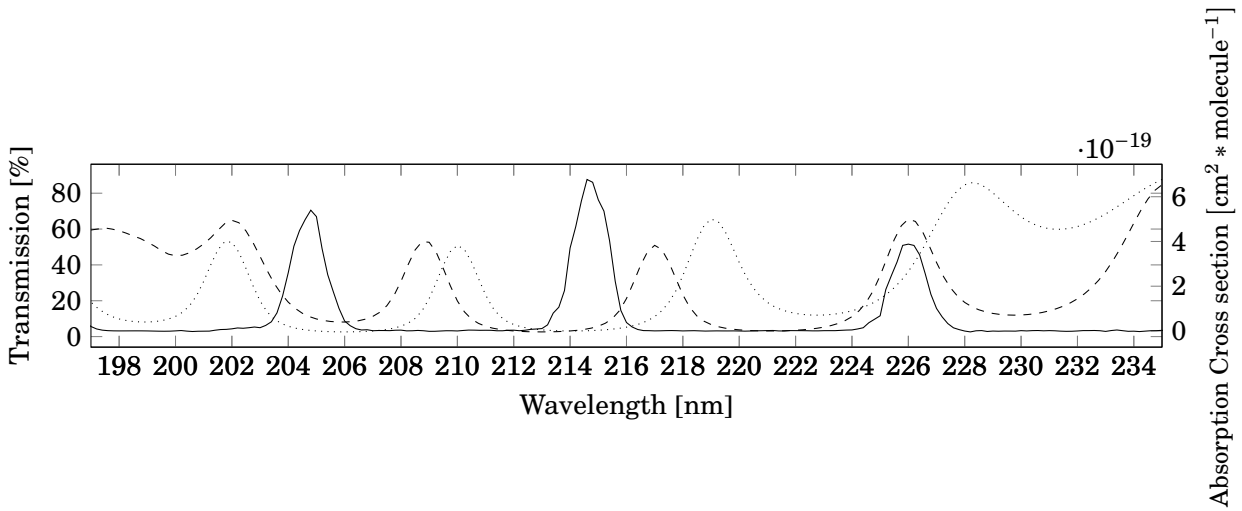


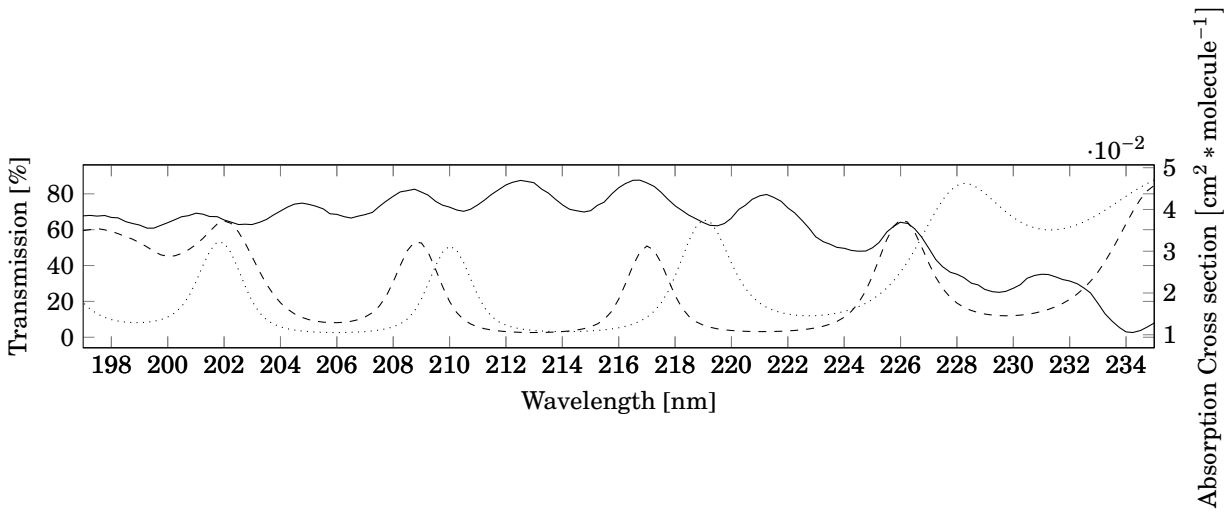
Figure 2.21: Schematic drawing of the etalon with a horizontal incident beam. The view is from above. d is the thickness of the substrate, β the deflection of the etalon to the normal placement perpendicular to the incident beam and x the path of the light through the etalon.

2.5.1 Etalon comparison

As the cost for the custom fabrication process is nearly the same for a few different etalons as for a single one, different etalons were made. These different etalons have quite similar properties, hence there are a little bit different and should give varying results. To have a reference for later discussion transmission lines of two etalons are plotted in the figures 2.23 and 2.24. In those two figures the small range in which the etalons work is clearly visible. This is due to the dielectric multilayer coatings which are working as partial reflectors and give sharp transmission peaks.



(a) NO Absorption Cross section and the etalon transmission peaks



(b) NO₂ Absorption Cross section and the etalon transmission peaks

Figure 2.22: The transmission spectrum of the etalon 5 (c.f. figure 2.23) perpendicular (dashed) to the incident beam and with a deflection of 20° (dotted). Overlaying the absorption cross section of NO (a) and NO₂ (b) (solid).

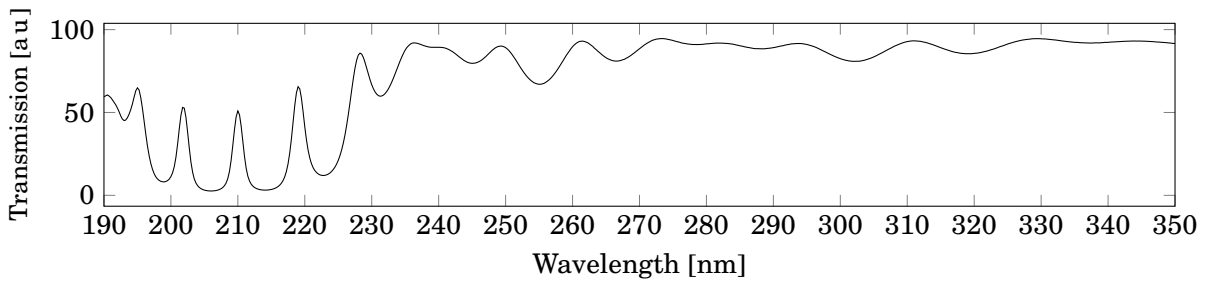


Figure 2.23: Transmission lines of the Etalon 5. This etalon should give the best results when taking the absorption spectrum and the filter into account.

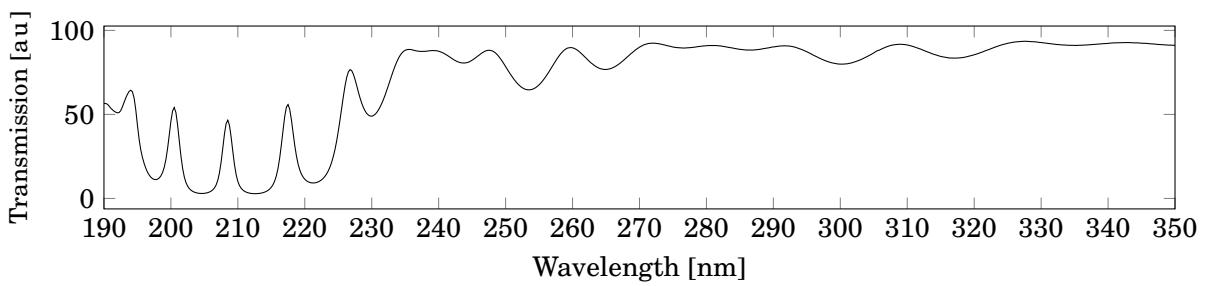


Figure 2.24: Transmission lines of the Etalon F.

EXPERIMENTAL

This section describes the used parts for both experimental setups. The specific parameters are stated in results and discussion.

3.1 Absorption spectroscopy

3.1.1 Concept

As the function of the setup has to be non-dispersive it is not possible to use a spectrometer to check the light intensity at a specific wavelength. Therefore the sensors are always illuminated by the full spectrum. This means there is no selectivity for a specific gas, the signal will decrease as long as the medium absorbs anywhere in the spectrum. In order to have a selectivity it is necessary to have some special part (one possibility is a filled NO gas chamber which will interfere with some parts of the spectrum) in the setup. This special part was in our setup the etalon, which was specific made to best fit the absorption lines of NO (see section 2.3.2). The signal will change when the transmission lines of the etalon match the absorption lines of NO. With the usage of two detectors (see figure 3.2), which are illuminated by light with different path lengths in the absorbing medium, the signal is a difference signal (c.f. equation 3.1), so the signal will increase when the transmission lines and absorption lines match.

$$(3.1) \quad \textit{Signal} = \frac{\textit{Signal Sensor 2} - \textit{Signal Sensor 1}}{\textit{Signal Sensor 2}}$$

3.1.1.1 Etalon concept in theory

All parts of the absorption setup (c.f. figure 3.2 and figure 3.3) except for the etalon and the detector board with the photodiodes are commercially available. The etalon is specifically made and has transmission lines matching the NO absorption peaks (c.f. section 2.5). Sweeping the etalon from the position with minimal overlay (overlay meant as matching the transmission peaks to the absorption peaks) to the maximum overlay leads to an increase of the signal when NO is in the flow cell. This method is possible due to distinctive, equidistant absorption peaks of NO and the constant absorption spectrum in the wavelength range of these peaks from all other expected gases (c.f. section 2.3.3 and section 2.3.4). The transmission spectrum of the etalon is made to match those NO absorption peaks as good as possible. Therefore only light with specific wavelengths will pass and enter the flow cell. If the etalon is deflected in a way that the transmission peaks do not match the absorption peaks the light intensity will not be reduced by absorption of NO, therefore the signal will be nearly the same on both detectors (c.f. figure 3.2). Deflecting the etalon to a position where the transmission lines let light pass with the wavelength in the area of the absorption peaks (the transmission peaks and the absorption peaks overlap as good as possible) the signal on one detector will be decreased more due to absorption of NO than for the reference detector. As the signal is calculated according to equation 3.1 this leads to an increase of the signal. For other gases like the expected NO₂, nitrogen or aromatic hydrocarbons the signal will not change very much when turning the etalon due to the nearly constant absorption of those gases in the wavelength range, which is limited by the filter in the setup.

3.1.2 Experimental setup

The light of a Xe-flash lamp, Hamamatsu L9455-13, is collimated with a lens (Thorlabs LA4936). The spectrum of the light source and the attached fibre are shown in figure 3.1. The light path is through a tilted filter (Peak at 214 ± 3 nm, FWHM 22 ± 4 nm). After the filter the light passes through the Fabry-Pérot etalon (cf. section 2.5) which is custom made from LayerTec. It is mounted on a rotation stage with a one degree scale.

After the etalon the beam is focused with another lens (Thorlabs LA4130) and routed through a fibre and collimated with a lens. As a sample chamber a glass-cylinder from Starna is used with an inlet and an outlet, optical path length 10 cm. After the glass-cylinder two sensors, on a custom detector board with a possible preamplifier, are placed next to each other. One is directly illuminated by the beam, therefore the light passes once through the gas filled flow cell. The beam for the second detector is reflected by two UV-enhanced aluminium mirrors from Thorlabs back into the cell and on the detector, in sum three passes in the absorption medium. Around the setup a box was built to reduce the noise level of stray light from the room.

To control the gas flow through the cell a mass-flow controller is used to mix synthetic air, N₂ and 400 ppm NO/NO₂, all gases were purchased at LindeGas. The carrier gas for NO is N₂, for NO₂

it is synthetic air. In all measurements a constant flow of 1000 ml/min is used. To record the data a Red Pitaya is used with a custom firmware.

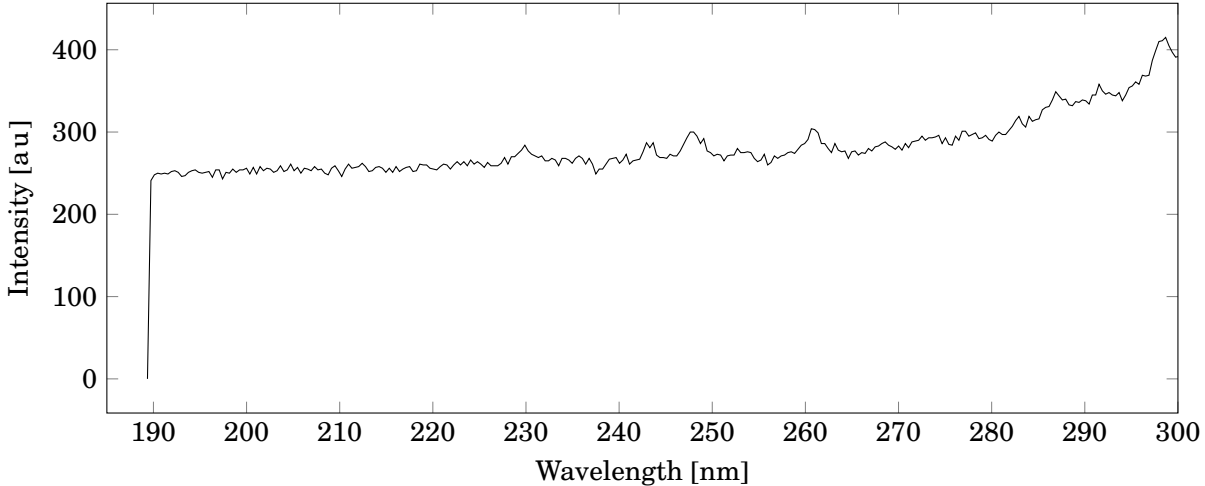


Figure 3.1: Spectrum of the used Xe-flash lamp when transmitted through the fibre, which is used to couple it into the setup. The spectrum is only shown up to 300 nm because the used filter has a transmittance only in this area.

Advantages of using two detectors When using two detectors and calculating the difference of the two signals it is possible to get rid of interferences or variations of the light source and in the light path. Variations of the light intensity would add to the noise if only one detector is used.

3.1.3 Custom made absorption cell

As this thesis is part of a project at the CTR AG some tasks were performed by other team members. One task was the design and calculation of a custom made absorption cell. The design was calculated with the program Optical Studio of Zemax. The idea was to get a more stable prototype with fixed mirrors and lenses, which focus the beam onto the sensors. With the focused light and the increased path length to 15 cm the signal-to-noise ratio should increase e.g. a higher resolution for measurements. Another advantage of a stable prototype is the elimination of scattered ambient light. The absorption cell is a milled aluminium block with an inlet and the outlet on the two ends. On one end the coupling for the light is mounted with an attachment, where the lens is installed. This attachment is held in place with screws and gas tight with seals and a window. The detectors are mounted outside of the cell with a frame onto the aluminium. In front of each detector a lens is mounted to focus the light. On the lens for the first detector a mirror is glued onto to reflect the light onto another mirror and then onto the second detector.

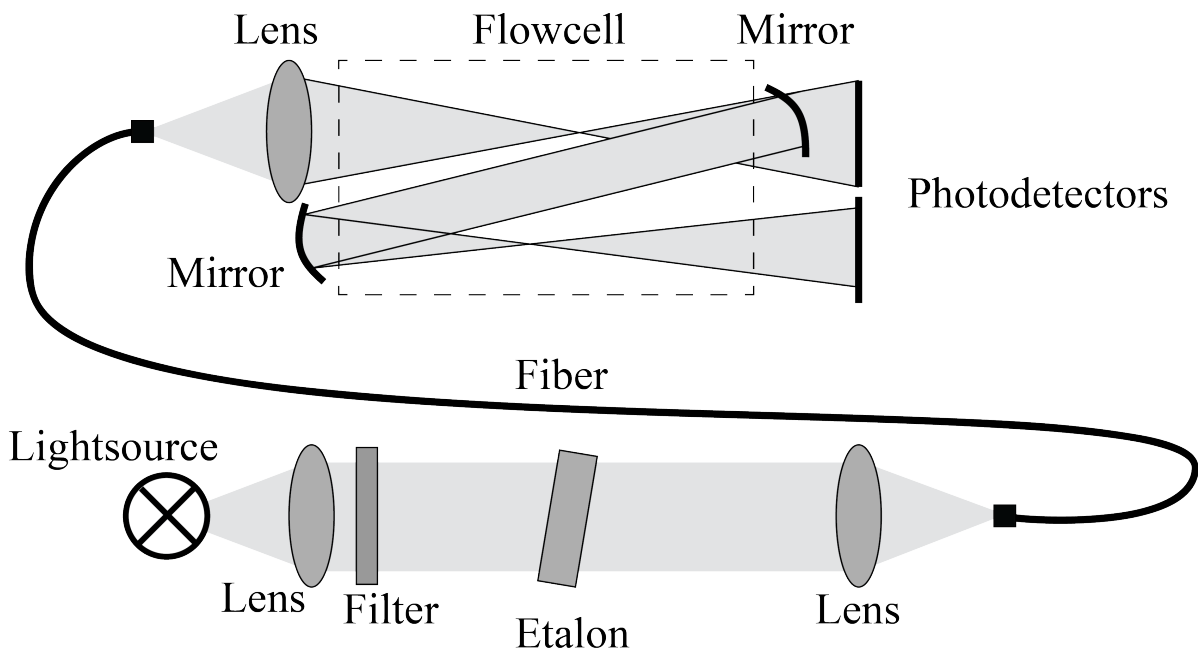


Figure 3.2: Setup for the absorption measurements for the manual turning of the etalon. The spectrum of the filter is shown in figure 3.6. A picture of the real setup is shown in figure 3.3

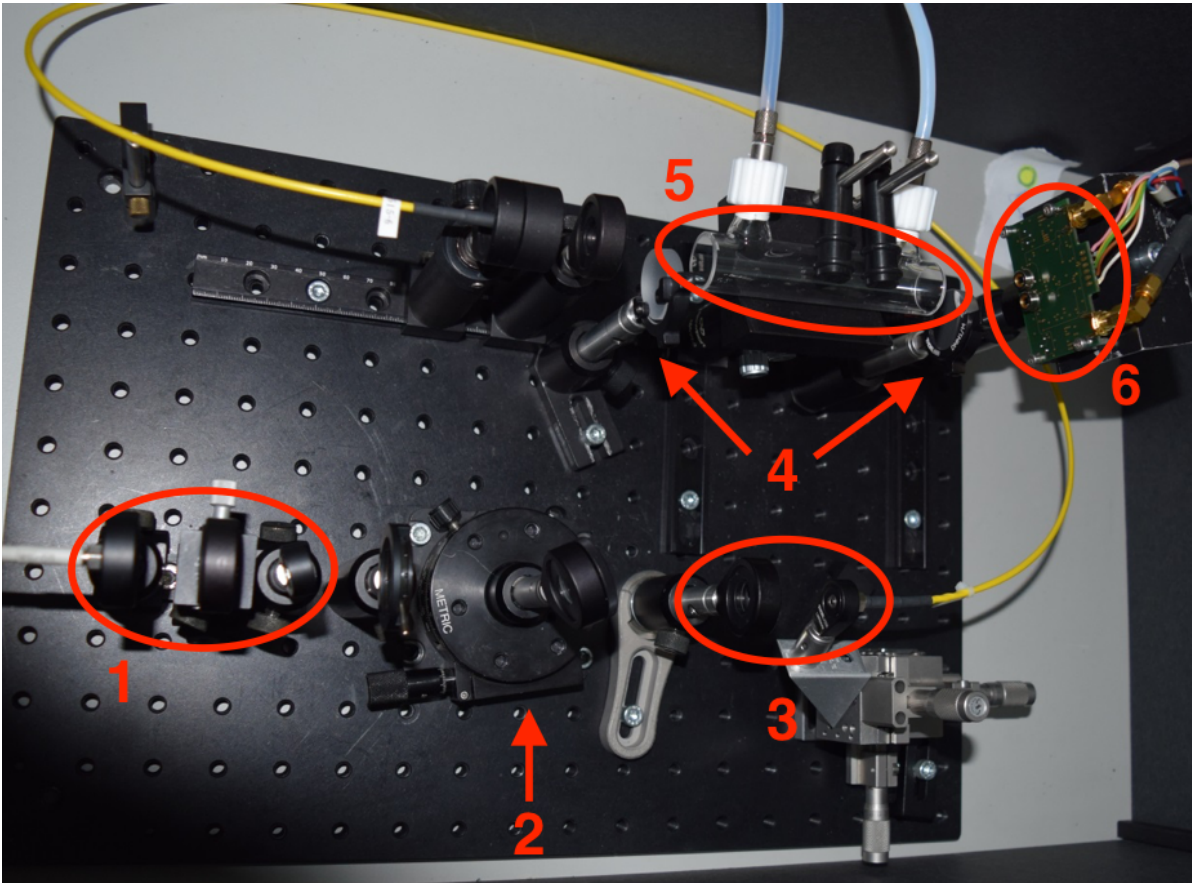


Figure 3.3: Setup for the absorption measurements for the manual turning of the etalon. The schematic setup is shown in figure 3.2. Around the setup a shielding was built to reduce the noise created by stray light in the room. 1: Light in coupling with the first lens and the tilted filter; 2: Etalon, mounted on rotation stage; 3: Second lens and in coupling into fibre; 4: Mirrors; 5: Flow cell; 6: Detector board with two sensors;

3.2 Fluorescence spectroscopy

For the measurements of fluorescence the same light source as for the absorption is used. The beam is collimated with a lens, passes through the filter used in the absorption setup and through a flow-cell (Starna 46-F/Q/10). The usage of the lamp, filter and lens of the absorption setup is due to reasons of simplicity and costs. A concave mirror, made of UV-enhanced aluminium purchased at Thorlabs, perpendicular to the incident beam reflects the fluorescence light of NO through a filter and a two-lens system, 2 times a Thorlabs LA4052, and on a photomultiplier tube. The used photomultiplier tube is a Hamamatsu R943-02.

The filter for the fluorescence light is a filter with a peak wavelength of 265 ± 3 nm and a FWHM of 25 ± 5 nm. As the lamp and the filter for the incident light were predefined the second filter was chosen at this wavelength and FWHM to cut off the incident light and reduce the noise by detecting scattered light. On the other hand the filter has to have a transmittance for the fluorescence light (c.f. section 2.4.3). In figure 3.6 the spectra of the filters are plotted.

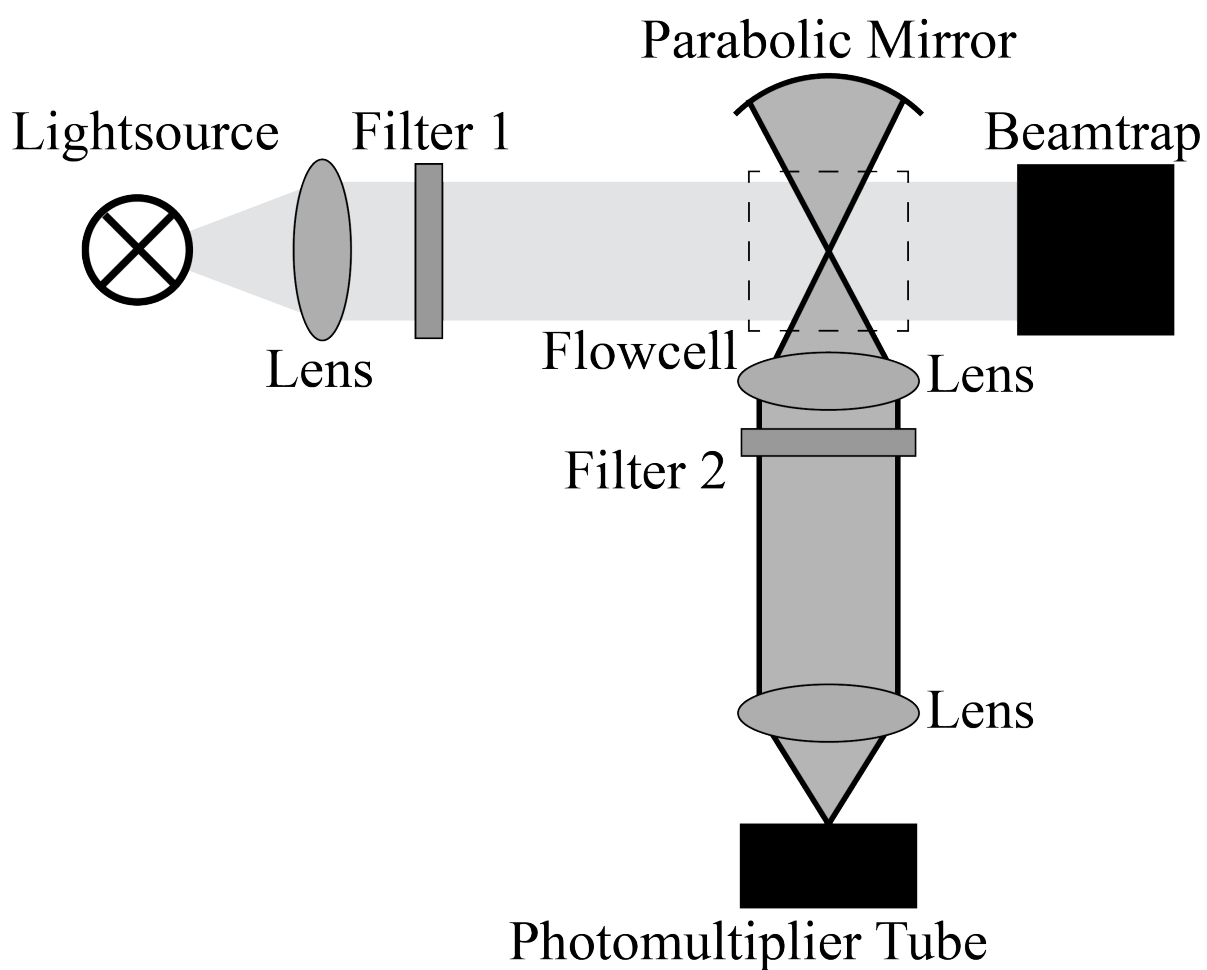


Figure 3.4: Schematic setup for the fluorescence measurements. The transmission spectra of the filters are shown in figure 3.6.

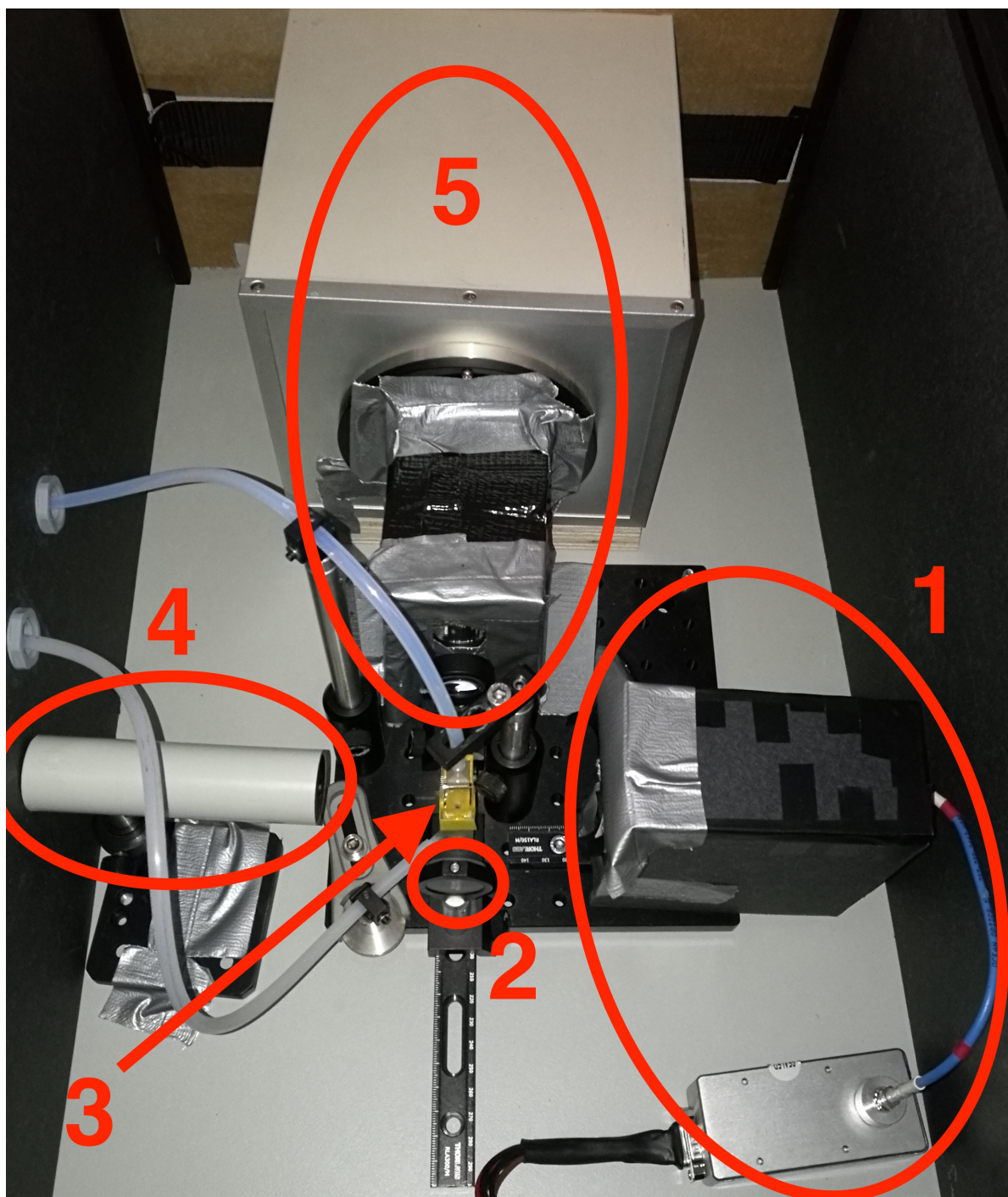


Figure 3.5: Setup for the fluorescence measurements. The schematic is shown in figure 3.4. 1: Light coupling with shielding, same as for the absorption setup; 2: Concave mirror; 3: Flow cell; 4: Beam trap to reduce stray light; 5: Fluorescence light path with two lenses, a filter and the photomultiplier tube; As for the absorption setup a shielding was build to reduce the stray light.

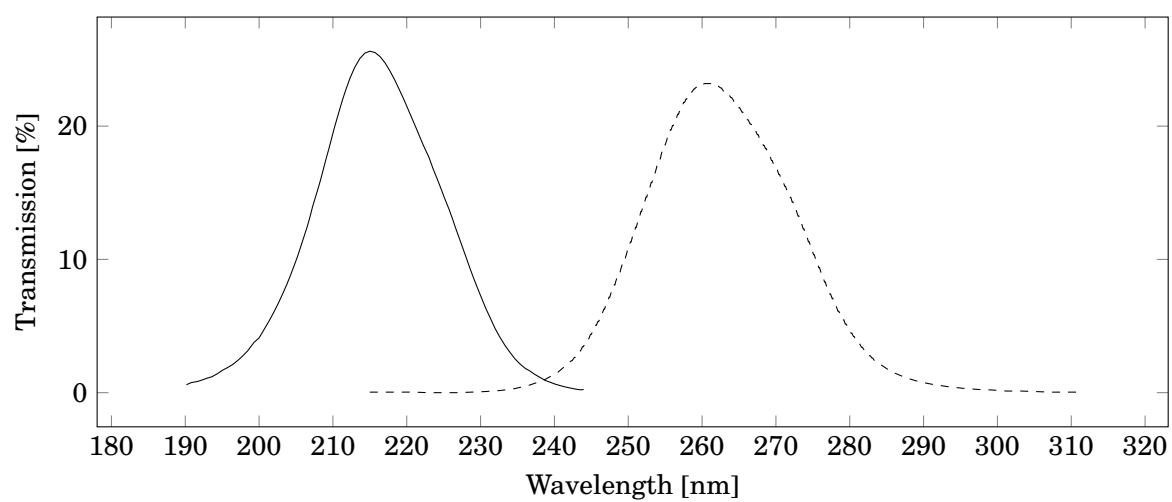


Figure 3.6: Real filter values before (Filter 1 in figure 3.2 and figure 3.4) and after the fluorescence cell (dashed, Filter 2 in figure 3.4). The second filter cuts off scattered light.

RESULTS AND DISCUSSION

Main part of this thesis was to check the usability of the two concepts and get a first premonition for the possible resolution. This chapter summarizes the results and an interpretation is given.

4.1 Mass flow controller

As stated in the chapter 3 mass flow controller were used to mix the desired ratios of NO/NO₂ with synthetic air or N₂. These were tested beforehand and they showed deviations in the lower ranges where the gas flow is reduced to small rates. These tests suggest a reference measurement before or after the flow cell to get a more detailed analysis. Unfortunately these reference measurements were not possible when doing the following investigations. Mentioned concentrations are referring to the test gas (NO or NO₂).

4.2 Fluorescence measurements

An idea to evaluate the concentration of nitric oxide in a gas sample is the measurement of light induced fluorescence, e.g. using UV-light in the range of 200 to 230 nm to excite the molecules and measure the fluorescence in the range of 250 to 280 nm (a more specific view of the emission and fluorescence range see figure 3.6). The trigger for the flash lamp is used as trigger for the oscilloscope to start the acquiring of the data. The signal is recorded as function of time. It later can be used to calculate the exponential decay of the fluorescence light.

The flash lamp frequency, and therefore the repetition rate, for the fluorescence measurements was 1 Hz. The background light intensity measured with synthetic air in the flow cell (cf. section 4.2.2) was subtracted from all measurements except for the first two subsections.

4.2.1 Dark measurements

To check the dark count from the photo multiplier tube (PMT) a measurement with the lamp disconnected from the power source was performed. The intensity-time diagram is plotted in figure 4.1. 116 shots were recorded and the mean value was calculated and is $(135.5 \pm 0.2) \cdot 10^{-6}$ V.

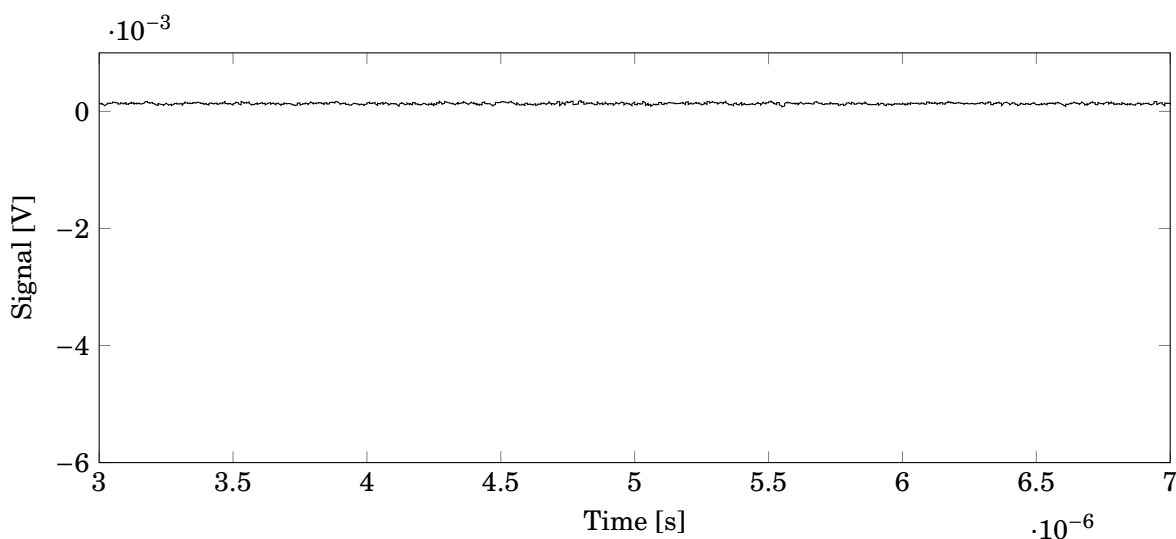


Figure 4.1: The dark signal with the lamp disconnected from the power source. The background signal level from the PMT has a mean value of $(135.5 \pm 0.2) \cdot 10^{-6}$ V, calculated from 116 shots.

4.2.2 Measurements with synthetic air

The first measurement was done with synthetic air in the flow cell to get the intensity from the background light as there is no fluorescence expected. As seen in figure 4.2 the intensity of the background light is clearly visible. This peak will be subtracted from the following results before further analysis. 109 shots were recorded.

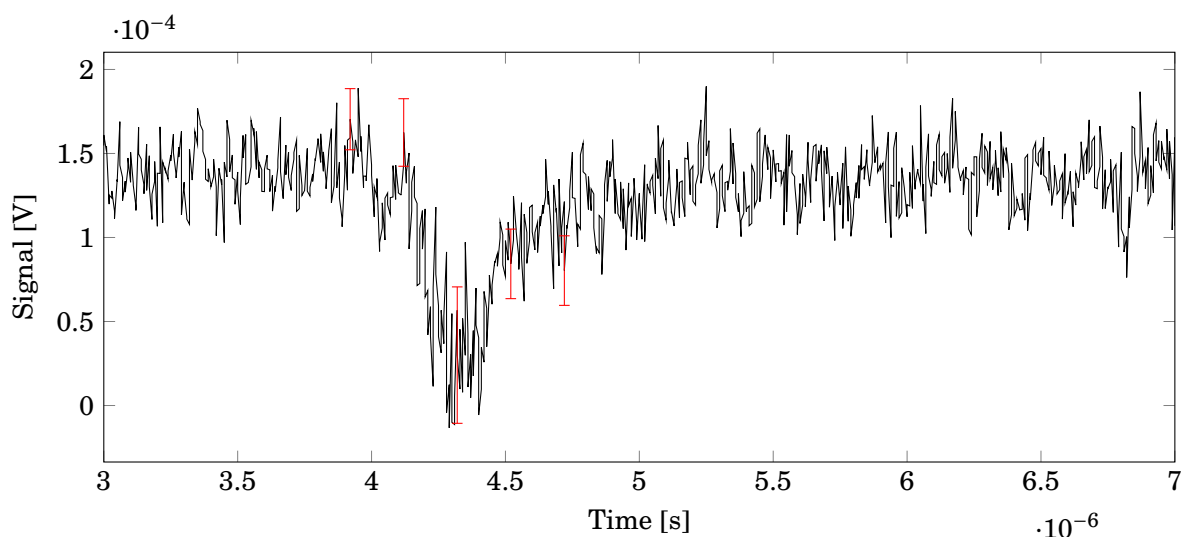


Figure 4.2: Measurement for the fluorescence intensity when the flow cell is flushed with synthetic air. As there is no fluorescence expected it gives the background light intensity. Note: This plot has a different y-axis scaling.

4.2.3 Nitric oxide and nitrogen

When flooding the flow cell with 400 ppm nitric oxide with a flow of 1l/min leads to a clear visible fluorescence. Diluting nitric oxide with nitrogen decreases the intensity linear with the dilution (cf. figure 4.3) in agreement with Okabe et. al in [21]. For the figure 4.3 the mean values of all samples for each concentration were calculated, sample size according to table 4.1. Integration over each peak and taking the mean value for each concentration leads to a nearly linear decrease with dilution (cf. figure 4.4), this was expected since it is already investigated by [27]. This dependency shows that the setup generates fluorescence and quantitative measurements are possible.

Table 4.1: Number of measurements for the NO/N₂ investigation, concentrations given for NO.

ppm	samples
5	102
10	113
50	101
100	117
200	104
300	108
400	112

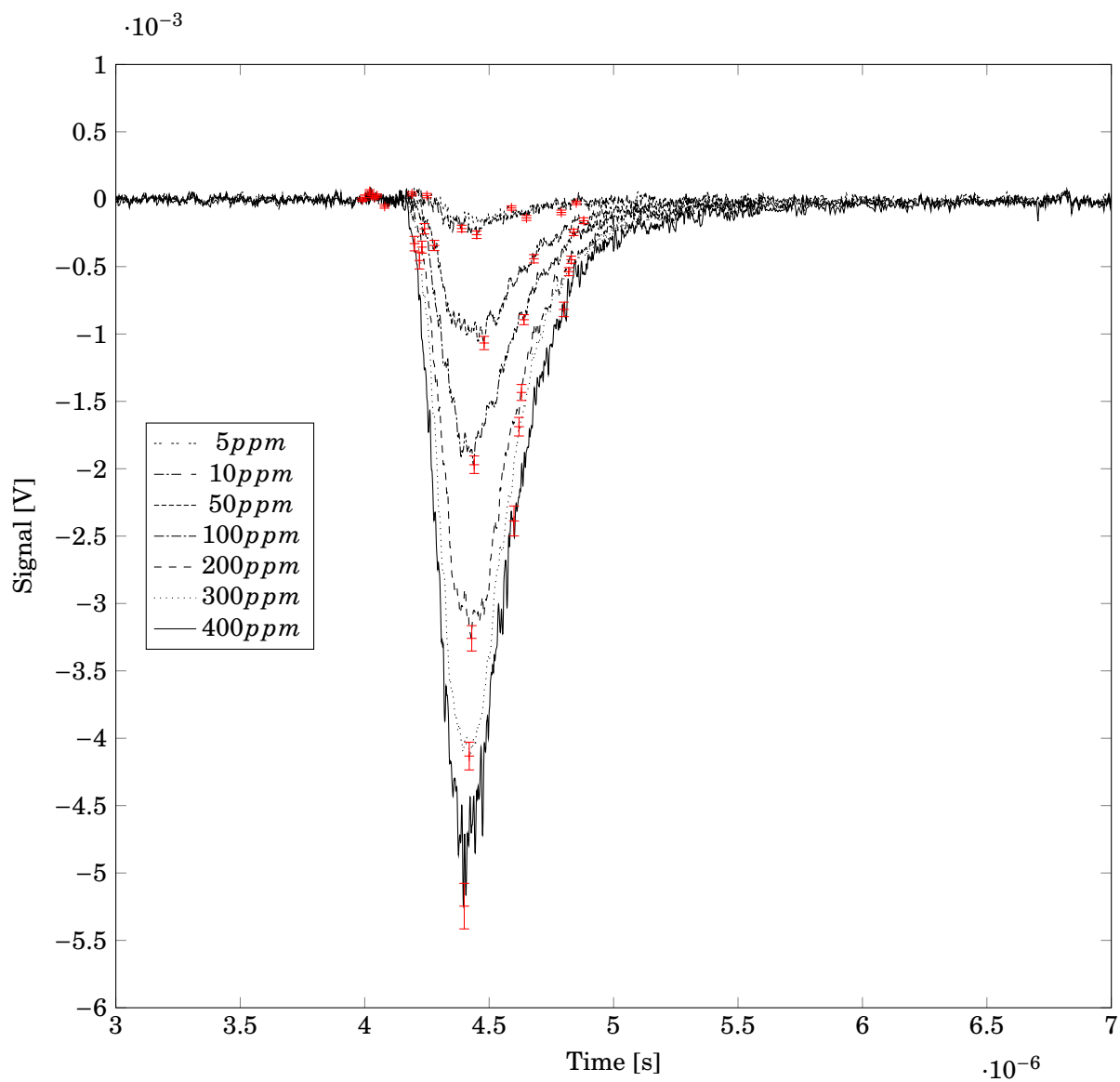


Figure 4.3: The mean fluorescence signal for different NO and N₂ ratios, as expected the signal increases nearly linear with the amount of nitric oxide. The integrated signals depending on the concentration is shown in figure 4.4. Error-bars indicate the standard deviation of the signal.

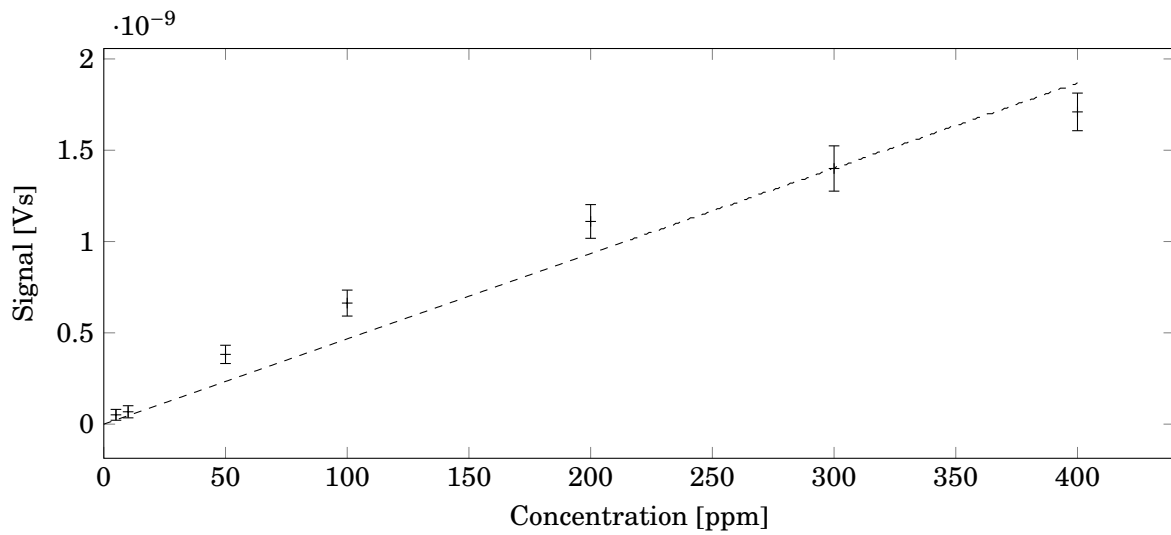


Figure 4.4: Integration of the different NO fluorescence signals yields to the nearly linear dependency. The absolute value of the integrated signal is shown averaged over all measurements, error-bars indicate the standard deviation for a single shot. The data was linear fitted. The number of measurements is depicted in table 4.1.

4.2.4 Nitric oxide and synthetic air

In the literature a strong quenching effect is investigated for the nitric oxide fluorescence when mixing it with small amounts of CO_2 . This effect can be compensated by a dilution with nitrogen. As air consists mainly of nitrogen and oxygen the influence of air on the fluorescence was a point of interest. The intensity for different nitric oxide - synthetic air mixtures are shown in figure 4.5. In table 4.2 the number of samples is given. In comparison to the results for dilution with nitrogen a strong quenching effect is visible attributed to the oxygen. The quenching of the intensity is more than a factor of 10. The absolute signal intensity is given in 4.7. In comparison to the linear behaviour for a dilution with N_2 (c.f. figure 4.4) a clear non-linear behaviour is observed. When decreasing the quencher concentration the signal increases significant. Due to the strong quenching by the contained oxygen a dilution of the exhaust gas with air to counter the quenching of CO_2 is not possible. The dilution with molecular nitrogen could be considered since it is investigated in the literature [21] but it is not suitable for a mobile measurement system. A stationary device could also use the expansion into a vacuum chamber which would act as dilution but additionally reduces drastically the rate of molecular collisions due to the cooling upon expansion. To determine if this type of dilution is effective, further investigation is needed.

Table 4.2: Number of measurements for the NO/synthetic air investigation, concentrations given for NO.

ppm	samples
10	108
50	107
100	104
200	108
300	111

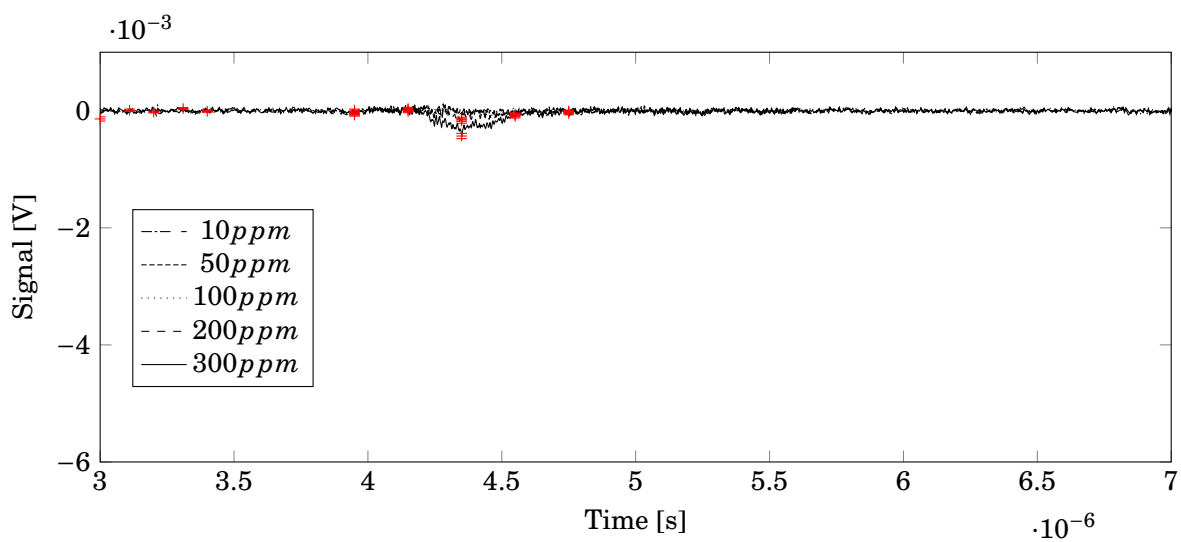


Figure 4.5: Mean fluorescence signal of different ratios of nitric oxide and synthetic air. In figure 4.6 the data is plotted with a changed y-axis to show more detail. Error-bars indicate the standard deviation.

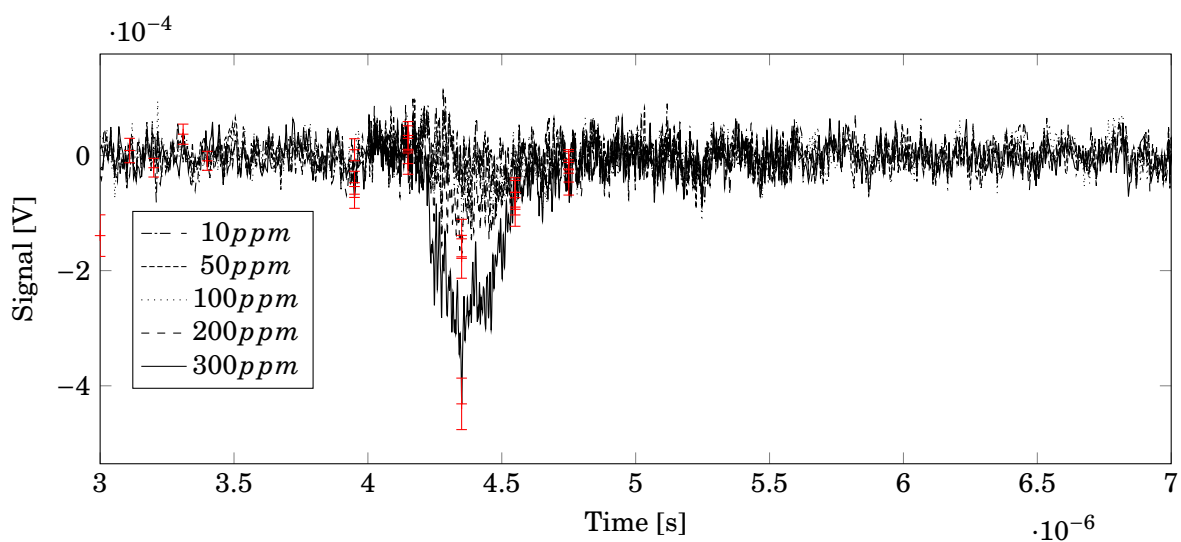


Figure 4.6: Data from figure 4.5 plotted with a different y-axis scaling for more detail.

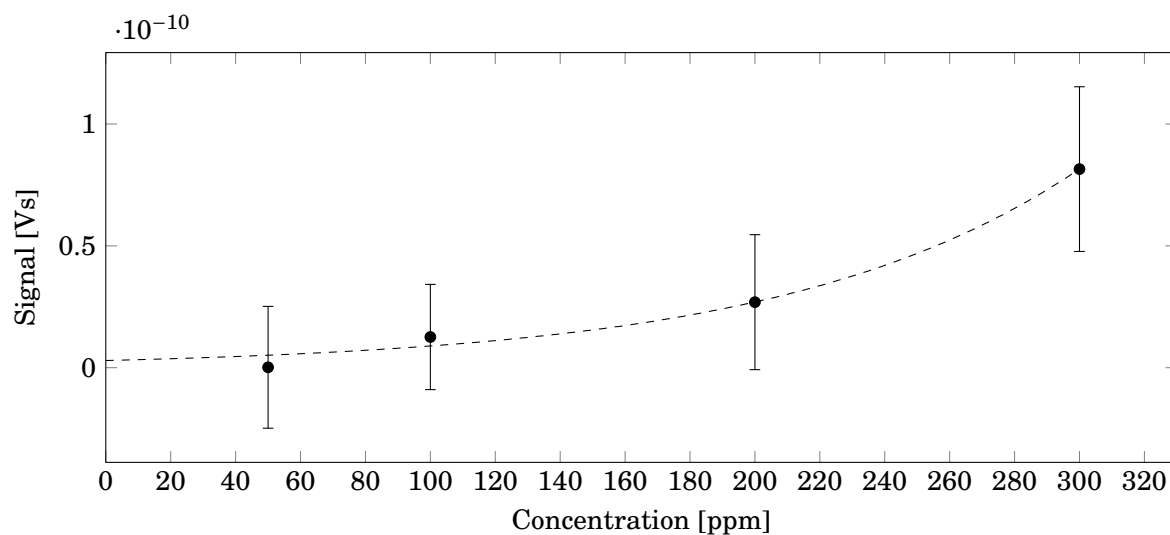


Figure 4.7: Absolute signal intensity for the NO-fluorescence when diluted with synthetic air (for signal-time plot see figure 4.6) integrated and plotted depending on the concentration. Error-bars indicate the standard deviation for a single measurement. Fit function (dashed): $y = A_0 \cdot \exp(x/t)$

4.2.4.1 Quenching rate

With the integrated intensity of the quenched fluorescence and the fluorescence without quencher a Stern-Volmer plot can be plotted. This plot should give a linear dependency between the two intensities. The slope of the linear fit gives the Stern-Volmer constant K_{SV} (c.f. section 2.4). Ideal the fit intersects the y-axis at 1 (or 0 if $(I_0/I)-1$ vs concentration is plotted). The bimolecular quenching constant is the Stern-Volmer constant K_{SV} divided by the lifetime.

This method does not lead to satisfying results for our measurements. Comparing the experiments done with some in literature leads to the conclusion that our NO concentration is too low to calculate the quenching rate for O_2 . This means that the data in section 4.2.4 is always too strong quenched for an evaluation respecting the quenching rate with a Stern-Volmer Plot.

A second try to calculate the quenching rate was made by fitting every result to a single exponential decay function and getting the mean value for the decay time for each concentration. Plotting the concentration vs. the reciprocal of the decay time, the decay rate constant, should lead to a linear dependency. The decay rate constant k' is the sum of the quenching k_q and the rate coefficient of the radiative loss k_r , c.f. equation (4.1). Plotting it against the concentration gives the two factors, the slope is the rate constant, the y-axis crossing is the factor k_q [8].

$$(4.1) \quad k' = k_r + k_q[Q]$$

Doing this analysis with the measured data does also not lead to a satisfying result because of the scattered light and the long pulse rate of the flash-lamp. The scattered light overlays with the decay of the fluorescence. Therefore the calculation of the lifetime is not possible. Concluding it is to say that for the calculation of the quenching rate the NO concentration was too low. Higher concentrations were not accessible, due to costs and toxicity. Furthermore higher NO concentrations would not be useful for the development of investigation methods for NO in exhaust gas because the expected concentrations are lower than 400 ppm (c.f. section 2.1.1).

4.2.5 Nitric dioxide measurements

The same measurements as for nitric oxide were done with nitric dioxide as test gas and nitrogen as dilution gas. For this measurements no fluorescence in the investigated wavelength range was expected because the filter between the flow cell and the photomultiplier tube will suppress the emitted light (cf. section 2.4.4.1 and figure 3.6). The mean intensity for 400 ppm, averaged over 109 shots, is plotted in the figure 4.8.

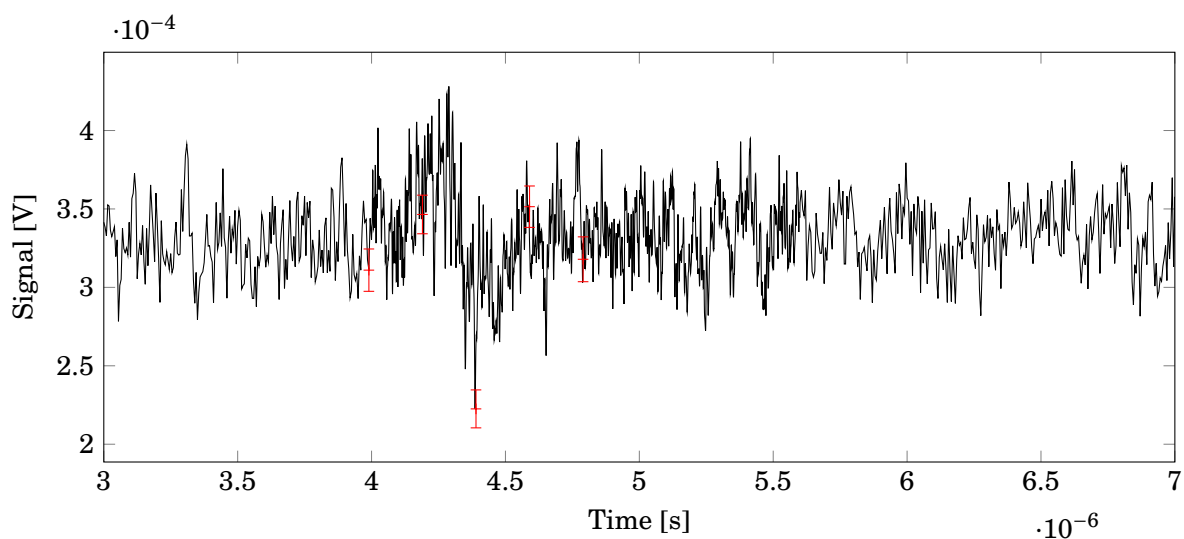


Figure 4.8: Fluorescence measurements with 400 ppm NO_2 as test gas. As expected no fluorescence was measured. Error-bars indicate the standard deviation of 109 shots.

4.2.6 Nitric oxide and nitric dioxide ratios

When mixing nitric oxide and nitric dioxide a strong quenching is observed (cf. figure 4.9). The quenching effect is the same as with synthetic air, this results from the fact that the carrier gas for nitric dioxide is synthetic air. Because of this circumstance the influence of NO_2 on the fluorescence of NO could not be investigated.

Table 4.3: Number of measurements for the NO - NO_2 measurements

ppm	samples
100	99
200	77
300	78

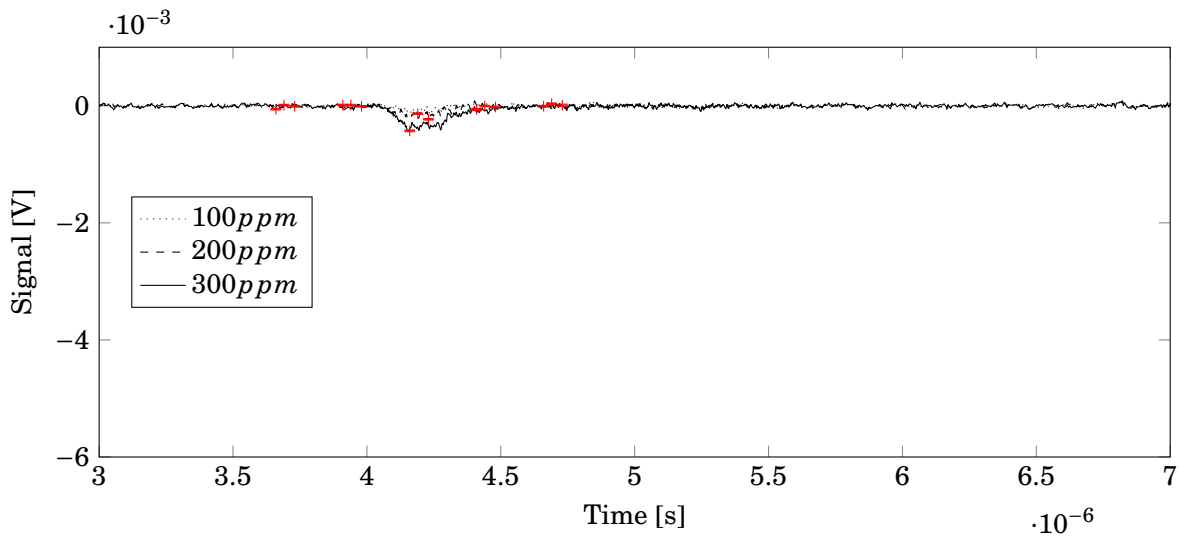


Figure 4.9: Fluorescence signal of different ratios of NO-NO₂ gas mixtures. In figure 4.10 the data is plotted with a changed y-axis to show more detail.

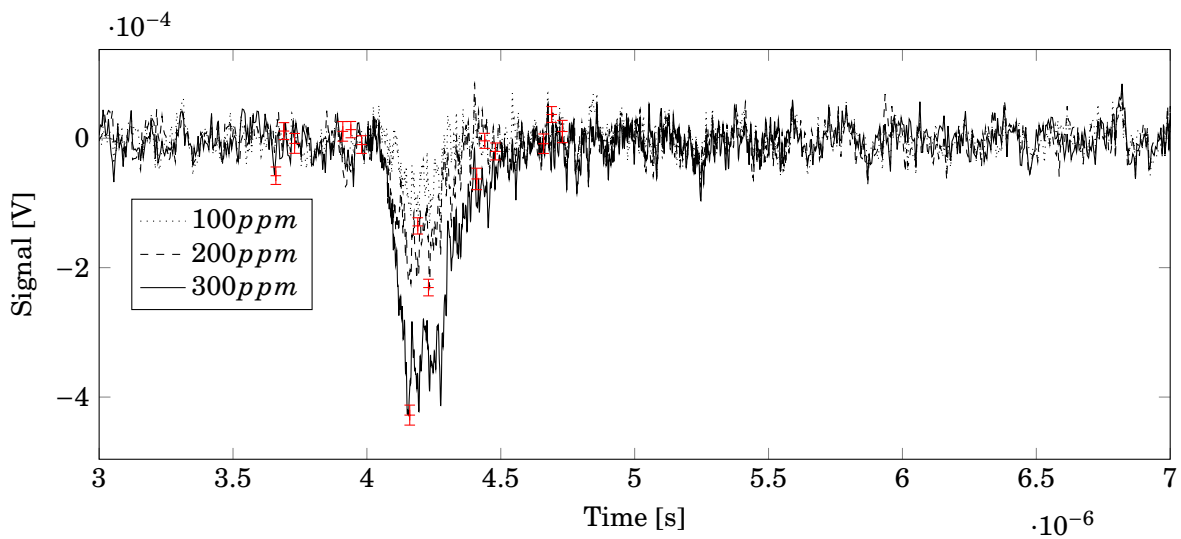


Figure 4.10: Data from figure 4.9 plotted with a different y-axis scaling for more detail.

4.2.7 Discussion of fluorescence measurements

A clear fluorescence of NO was measured using our setup and using a pure sample of the calibration gas. When diluting the gas with N₂ a linear signal dependency was investigated (cf. figure 4.3 and figure 4.4), this effect was stated in literature ([21], [27]). Dilution with synthetic air leads to a strong decrease of the signal due to the quenching effect of oxygen (cf. figure 4.5), which is also described in the literature [16].

As the mobile concentration measurement of nitric oxides in exhaust gas is the goal for this

project the quenching of O_2 is a deal breaker, although very low O_2 concentrations are expected. This is due the fact that the dilution with air was planned to cancel the strong quenching effect of CO_2 , which is a strong quenching gas (see section 2.4.3). Nevertheless the measurement method gives promising results for stationary measurements were a dilution with N_2 or an expansion into a vacuum chamber is possible. Specially when considering the low cross-correlations with other exhaust gases. Using the standard deviation with the pure NO sample to give an estimation for a measurement with a 500 Hz repetition rate leads to a standard deviation of $0.8 \cdot 10^{-4}$ V for a $-52.5 \cdot 10^{-4}$ V peak at 400 ppm.

4.3 Absorption measurements

Due to the negative results of the NO fluorescence measurements under the perspective to use it for mobile measurements of gas ratios in exhaust gas a different approach was chosen. Instead of using the fluorescence the absorption of nitric oxide is used for concentration measurement. To cancel the cross-correlations with other gases a custom made etalon and a specific data analysis (see section 4.3.2) is used.

In the following sections an angle value of an etalon deflection is always in relation to the angle of incident equal to zero degrees.

4.3.1 Influence of the Xe-Flash lamp on the calibration gases

The spectrum of the Xe-Flash lamp is shown in figure 3.1. The dissociation energy of NO is 6.55 eV [11] and therefore at a wavelength of 189.3 nm. For NO_2 the dissociation energy is 3.18 eV [11] i.e. 390.3 nm. This means the Xe-lamp emits photons with enough energy to dissociate NO_2 . So it is important to know how fast the lamp influences the NO and NO_2 concentrations and therefore the measurement.

With the help of a mirror the beam was directed into the cell, which was statically filled with 400 ppm NO_2 . Four UV-vis spectra were taken in an interval of 30 seconds, where the Xe-lamp was activated in between (Adding up to 90 s of exposure) with a repetition rate of 200 Hz. A 40 s gap was between the 4th and the 5th measurement. After the 5th measurement the exposure time was increased for the next three measurements to 60 seconds each. The last measurement was taken after another 300 seconds exposure. The total exposure time of NO_2 to the Xe-flash lamp added up to 640 s. The irradiance of the whole spectrum is $7.35 \mu W \cdot cm^{-2}$ (calculated in section 4.3.1.1), which is higher as expected for the absorption measurements because no filters were used for the influence measurements due to the compact setup.

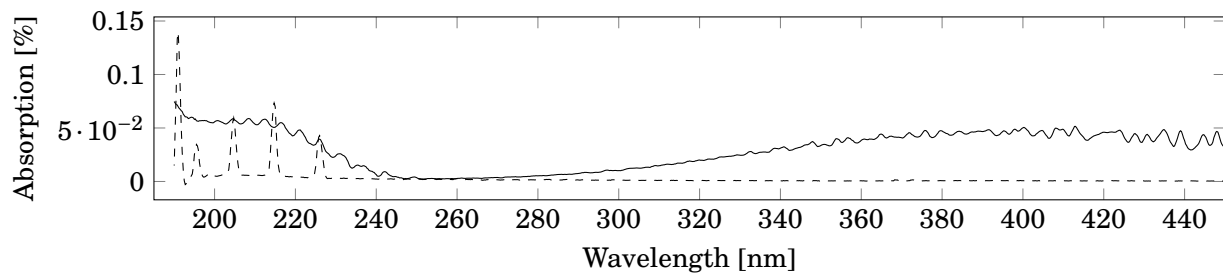
The experiment was redone with NO to investigate the influences of the Xe lamp. As there should be nearly no effect due to the high dissociation energy the exposure times were up to 1800 s (30 minutes).

Results The results for both experiments are plotted in the figure 4.11. In figure 4.13 the measurements are compared with the normal behaviour of NO_2 without the Xe-flash lamp because the spectrometer itself uses photons with higher energy than the binding energy e.g. influences the gas in form of photodissociation. Therefore we have an influence of the spectrometer itself. The same result is plotted with the time as x-axis in 4.13. In comparison to these measurements the Xe-lamp has some influence to the photo dissociation of NO_2 . The concentration of NO_2 decreases faster with longer exposure time of the Xe-lamp than without. This was expected since the lamp emits light with wavelengths with energy higher than the dissociation energy of NO_2 . With increasing illumination time the peaks of NO increase in the spectrum of NO_2 which is an indicator for a conversation due to the Xe-flash lamp. Specially the 214.4 nm peak increases over time (c.f. figure 4.12).

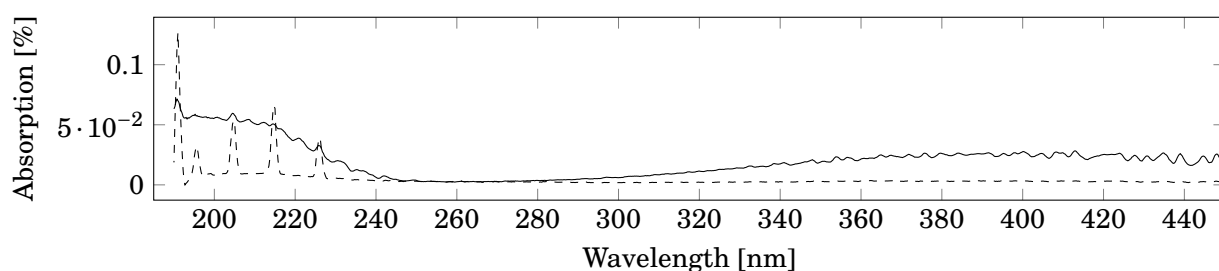
Although these results show clearly the expected influence of the Xe-flash lamp on the photo dissociation of NO_2 , the process is too slow to have an influence on the gas ratios during the measurements in the final setup and by continues gas flow. Considering a flow cell like the one used for these influence measurements with a length of 10 cm and a diameter of 3 cm, therefore a volume of around 70 cm^3 , a flow of 1 l/s will change the gas in the chamber with a rate of 14 Hz. Minimizing the diameter to 1.5 cm leads to a volume of around 18 cm^3 , and therefore to a gas change rate of 55 Hz for the same volume flow. This size of the flow cell correlates to the one used for further testing on the bread board.

The conversion will follow an exponential function, increasing with concentration. For the first few terms a linear behaviour is assumed, this leads to an average reduction of 1.26% for every 30 seconds, this results in a reduction of 5 ppm for the used 400 ppm. In a conservative way the assumption is made that the linear behaviour is still valid for the measurement done after 630 seconds of exposure. This would result in a reduction of 18.5 %, therefore 74 ppm for 630 seconds. This means a reduction of 3.5 ppm for an exposure of 30 seconds. This means for the desired resolution of about 1 ppm an exposure of 10 seconds is the critical threshold. As the conversion will slow down with lower concentrations due to the reduced possibility of a dissociation the conclusion is made that an exposure time of 30 seconds is not crucial for measurements with a resolution of 1 ppm in the range of the expected ratios (under 150 ppm, c.f. section 2.1.1 and table 2.2), specially when the fact is considered that the used filter will reduce the energy (transmission spectrum of filter see 3.6). An integration of 30 s results in a flow of $3.6 \cdot 10^{-2} \text{ l}$ per minute for a cell with 10 cm length and 1.5 cm diameter.

A look on the NO concentration reveals that the flash lamp has no visible effect on the gas. Therefore the influence can be omitted and do not have to be considered in the analysis.



(a) Spectrum of 400 ppm NO_2 and 400 ppm NO (dashed) before the Xe-flash lamp was activated



(b) Spectrum of 400 ppm NO_2 after 640 seconds and spectrum of 400 ppm NO (dashed line) after 1800 seconds of illumination with the Xe-flash lamp

Figure 4.11: Spectrum of NO_2 and NO (dashed line) with and without the Xe-flash lamp, the synthetic air background was subtracted. A detailed plot of the 3 spectra is shown in figure 4.12.

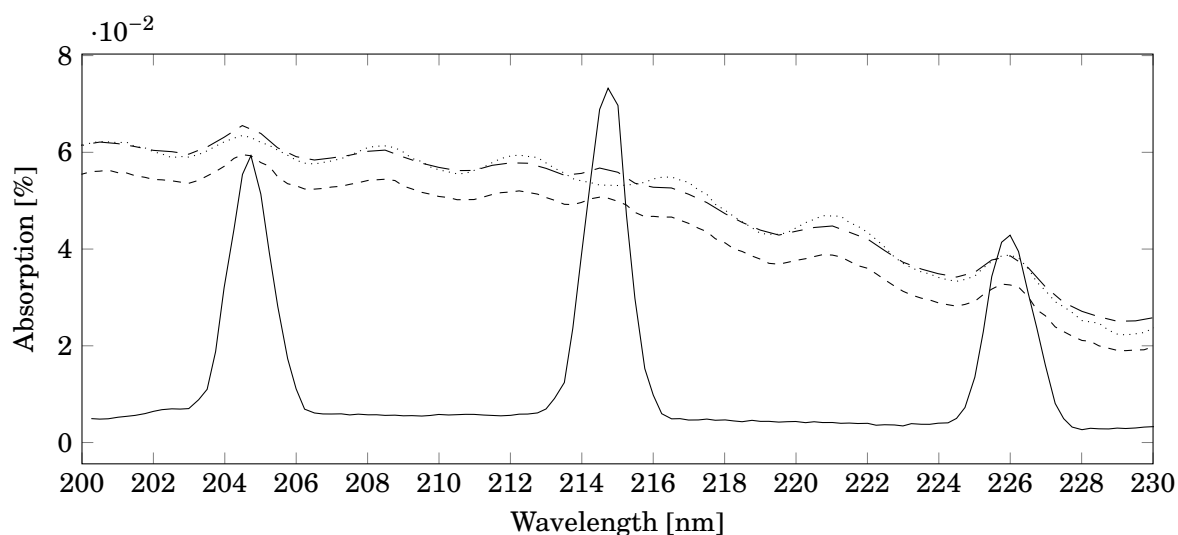


Figure 4.12: A more detailed view of the data in figure 4.11. To counter the reduction of the overall absorption the line for the 640 illumination was shifted up by the difference between the dashed and dotted line at 210 nm (dash pattern). Solid: NO absorption, dotted: 60 s illumination, dashed: 640 s illumination

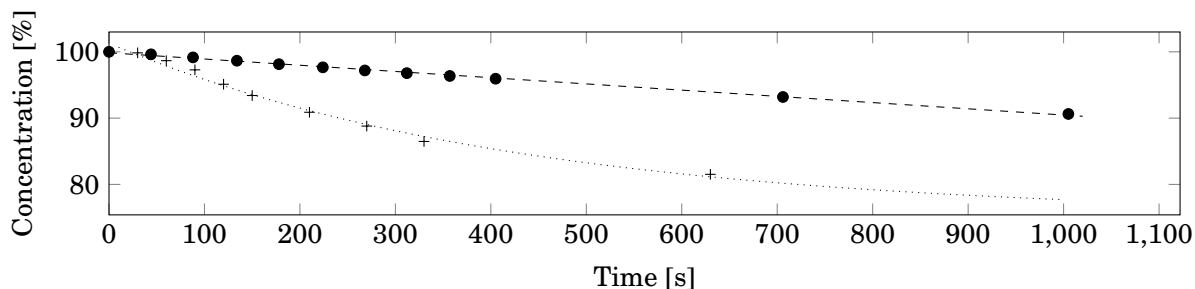


Figure 4.13: NO₂ Concentration behaviour over time, starting with 400 ppm. + marks show the concentration when the gas is additionally exposed to the Xe-flash lamp. The samples without illumination are linear fitted (dashed line). Fit function for samples with illumination (dotted): $y = y_0 + A \cdot \exp(-(t-t_0)/b)$

4.3.1.1 Pulse energy

In the datasheet of the flash lamp a plot can be found for the spectral distribution of a similar lamp (L9455-01, for the spectral distribution see figure 6.1 in the appendix). With the waveform difference of the main discharge capacitance (c.f. figure 6.2 in the appendix) in the datasheet of the two lamps the difference in irradiance can be calculated. With this data and the spectral distribution of the L9455-01 lamp the irradiance for the used lamp can be estimated. For the L9455-01 lamp the irradiance over the whole spectrum is $35.05 \mu\text{W} \cdot \text{cm}^{-2}$. The ratio L9455-13 to L9455-01 for the pulse of the main discharge capacitance is 0.2097. This gives a irradiance of $7.35 \mu\text{W} \cdot \text{cm}^{-2}$ for the used flash lamp.

4.3.2 Experimental approach and data analysis

This section explains how the data is analysed and what corrections or calibration procedures are applied before plotting the data. Before each measurement the flow cell is flooded with synthetic air. The data acquisition is started and the detectors are blocked to record the dark signal. This measurement is averaged and the two signals are corrected to the same level to correct the different offsets of the detectors. Afterwards a signal is recorded with synthetic air. This measurement is used to correct the different illumination and amplification by averaging over the data and correcting it again to the same level for both detectors. After this corrections the signal of the measurement detector S_2 is subtracted by the signal of the reference detector S_1 (for explanation why two detectors are used see section 3.1.2) and normalized (c.f equation 3.1).

4.3.3 Detection limit

4.3.3.1 Breadboard setup

For the analysis an important part is to know how the setup behaves at different concentrations. Therefore the gas cell was flushed with different gas ratios (400, 300, 200, 100, 50, 20, 10 ppm). The setup was operated without an etalon. The drift corrected signal is shown in figure 4.14. The signal does not show a linear response, e.g. the signal for 400 ppm is not a factor 20 higher than the signal for 20 ppm. This due to the saturation effect for the absorption. The flash lamp was triggered with 177 Hz. For a single shot the detection is limited to 50 ppm with a value of $(0.38 \pm 0.12) \cdot 10^{-2}$ and a signal-to-noise ratio > 3 . The next measured concentration, 20 ppm, has a mean value of $(0.22 \pm 0.12) \cdot 10^{-2}$ and therefore a signal-to-noise ratio smaller 2. The signal for 400 ppm is $(1.15 \pm 0.12) \cdot 10^{-2}$. For a one seconds measurement with 177 Hz the standard deviation decreases to $8.8 \cdot 10^{-5} \frac{1}{\sqrt{Hz}}$. This leads to a detection limit of around 2.3 ppm for measurement time of 1 second, considering a signal-to-noise ratio of 3 or higher.

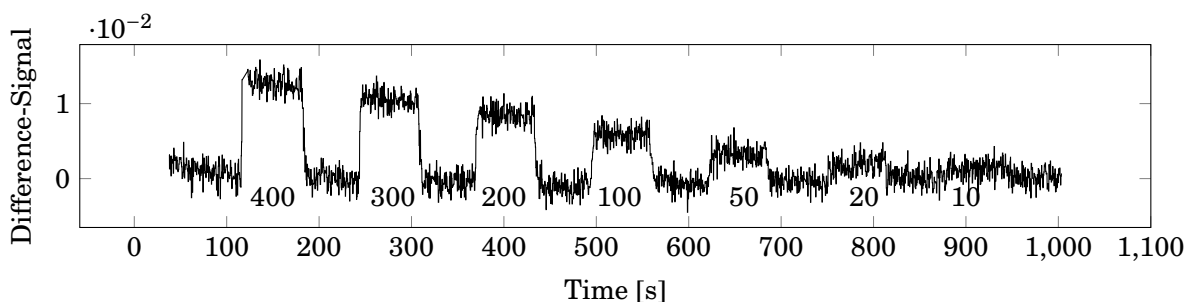


Figure 4.14: Measurement of the absorption from different NO ratios. Due to the noise of the bread board setup the detection limit is 50 ppm for a single measurement. The notes in the plot indicate the concentration for the steps in ppm NO. Standard deviation for a single shot with 0 ppm NO gas in the area of 186 s to 239 s: $0.12 \cdot 10^{-2}$.

4.3.3.2 Custom made measurement cell

In contrast to the bread board setup the measurement cell uses lenses right in front of the detectors to increase the amount of light illuminating the sensor. Therefore the expected signal to noise ratio should increase as the electrical amplification can be much lower. The measurement were performed in a similar way (repetition rate flash lamp 167 Hz, measurement for each ratio 65 s) as with the bread board setup although the chosen concentrations were 10, 50, 100, 200, 300, 400 ppm with 0 ppm in between. The measurement is shown in figure 4.15. The noise of the signal a little bit higher as for the bread board setup but the signal for the different concentrations is higher. In comparison to the measurement with the basic setup the signal for the 400 ppm is $(2.1 \pm 0.2) \cdot 10^{-2}$ with the measurement cell, comparing to $(1.15 \pm 0.12) \cdot 10^{-2}$ for the bread board setup). The detection limit is at 10 ppm with a mean value of $(0.6 \pm 0.2) \cdot 10^{-2}$ for a single

shot measurement. Calculating the standard deviation for a one second measurement with a repetition rate of 167 Hz for the flash lamp leads to a decreased standard deviation of $1.5 \cdot 10^{-4} \frac{1}{\sqrt{\text{Hz}}}$.

Calculating the detection limit for a one second measurement with a repetition rate of 177 Hz (same as for the bread board setup) leads to a value of around 0.7 ppm (again with a signal-to-noise ratio of 3). The increase of the signal-to-noise ratio, and therefore a decrease of the detection limit is mainly due to the longer path length of 5 cm (times 2 as the signal is a difference signal of 3 passes - 1 pass through the cell). Also the more advanced optical elements and the lenses in front of the sensors are a factor for the decrease.

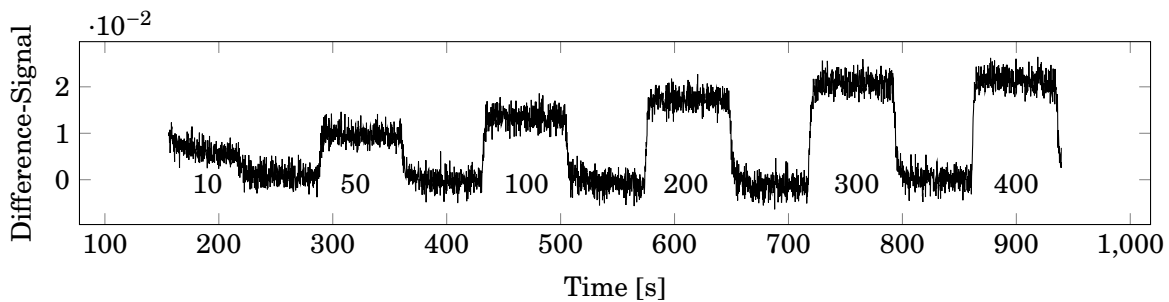


Figure 4.15: A similar measurement as for the bread board setup was performed using the custom made cell. In contrast to the result in figure 4.14 the noise is a little bit higher (Standard deviation for a single shot when 0 ppm NO gas is in the cell in the area of 218 s to 286 s: $0.2 \cdot 10^{-2}$) but the signal is stronger. The notes in the plot indicate the concentration for the steps in ppm NO.

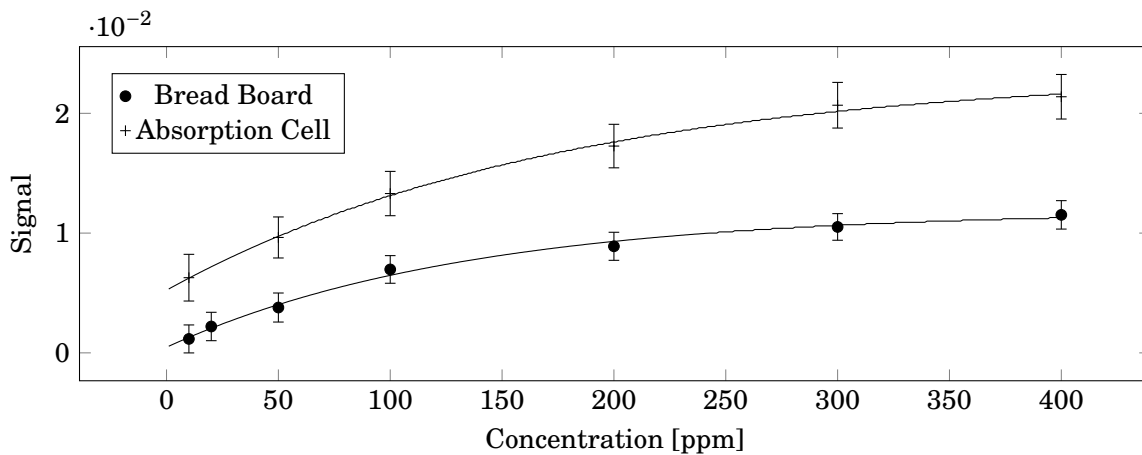


Figure 4.16: Mean values of the concentration steps for the bread board setup (c.f. figure 4.14, * marks) and the absorption cell (c.f. figure 4.15, + marks), Error-bars indicate the standard deviation for a single shot. Fit function $y = y_0 + A \cdot \exp(-x/t)$

4.3.4 Manual controlled etalon measurements

4.3.4.1 NO

The manual turning measurements were performed with the bread board setup. The etalon was mounted on a rotation mount. For every angle (0° to 25° in 1° steps) the spectrum of the source after passing through the filter and etalon was measured with an Ocean Optics USB spectrometer. This data was used to simulate the expected intensities for the different angles (cf. section 4.3.4.3). After the measurement for the simulation the dark current, the signal with synthetic air and the intensities with NO were measured. The dark current was measured for 20 s by detaching the light source, then the signal of synthetic air for 40 s and afterwards the cell was filled with 400 ppm NO and the signal was recorded for 60 s. These measurements were then dark current corrected and angle corrected for each angle using the synthetic air measurements. The angle correction is necessary due to the different reflectance of the mirrors for different wavelengths and the slightly different coupling into the fibre which changes the output beam-profile. After this adjustments the normalized mean value was calculated for the 60 s NO measurement. The results for different etalons are plotted in figure 4.17.

Results To get a high sensitivity the factor highest/lowest signal should be as high as possible and the signal to noise ratio should be as high as possible. In figure 2.23 the spectrum of the etalon with the best ratio is plotted. If the angle of incidence is 0° the whole contribution to the signal is from the 226 nm peak of the NO absorption. By turning the etalon the transmission spectrum is shifted (cf. section 2.5) and the peaks at 205 nm, 215 nm and 226 nm contribute with different intensities to the signal. Unfortunately the transmission spectrum of the etalon and the absorption of NO do not overlap ideally and therefore the signal is not as high as it could be theoretically (cf. section 4.3.4.3).

In comparison to the etalon F (for transmission spectrum see figure 2.24) the contribution at an angle of 0° is quite high. As the maximum signal is nearly the same as for the etalon 5 the overall factor maximum/minimum is worse. In consequence the possibility to separate the NO contribution to the absorption is less. For the highest/lowest ratio the first 3 values were taken for the lowest value to minimize the error due to low minimal values under the motive that the first degrees do not shift the transmission much.

4.3.4.2 NO₂

Using NO₂ as test gas the same measurements were performed as with NO (cf. section 4.3.4.1). In figure 4.18 the signal is plotted in dependency of the angle. Nitric dioxide can be used as example for all the other expected gases which overlap with the absorption lines of nitric oxide. Starting with a relative high intensity at 0° in contrast to the measurement with nitric oxide the signal strength stays nearly constant when deflecting the etalon to the 25° position.

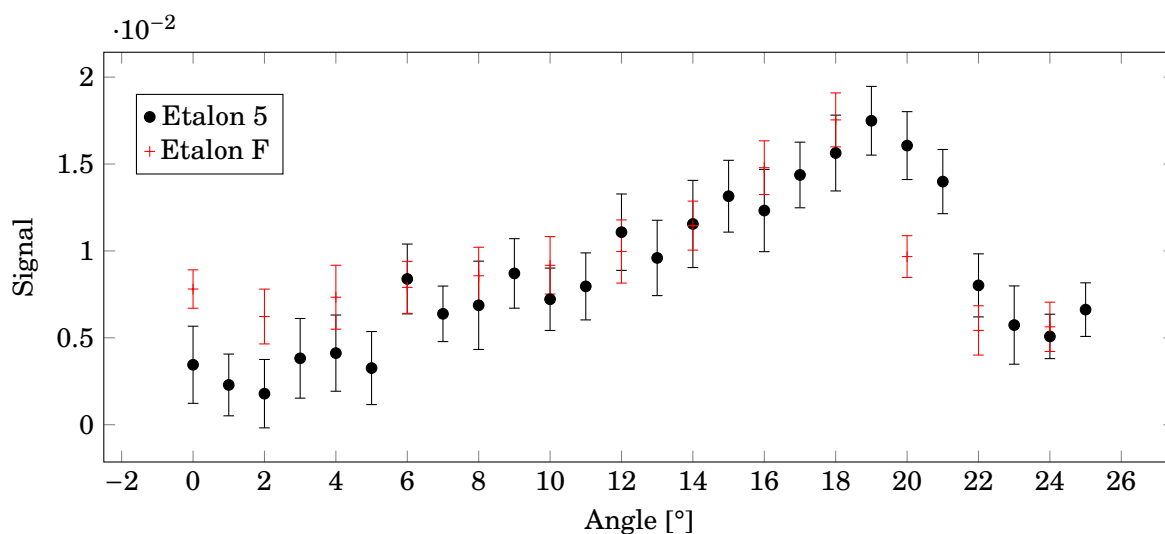


Figure 4.17: Signal strength depending on the deflection angle of the etalon 5 and for the etalon F with NO as test gas. The transmission spectra are plotted in figure 2.23 and figure 2.24.

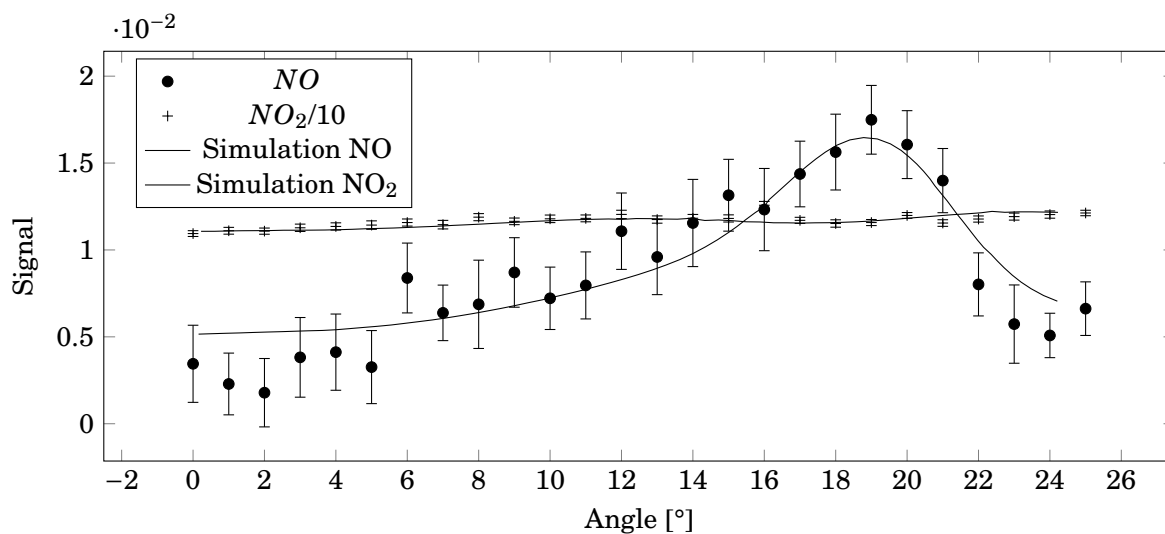


Figure 4.18: Signal strength depending on the deflection angle of the etalon with NO as test gas and NO₂. The used etalon was the etalon 5. The values for the NO₂ were divided by a factor of 10 to make a comparison more easy. The simulations are done with theoretical values match the measurements although a constant was subtracted to get a better match. Highest/lowest value NO: 3.2; Highest/lowest value NO₂: 1.1 The simulation was performed by Gerald Auböck at CTR.

4.3.4.3 Simulation and comparison

The data gained in the section 4.3.4 was used to calculate the expected intensity for each angle measurement using the Lambert Beer law (cf. equation 2.2) with the absorption coefficient of NO as ϵ . The calculated intensities were plotted angle dependent. The plot shows as expected an

increase in signal, which means a different intensity change at the detectors. In comparison to the actual measured data the peak and the factor highest/lowest value are shifted (cf. figure 4.18 and figure 4.19). A possible explanation for this is the unknown, possibly not linear, sensitivity of the spectrometer. An intensity calibration of the spectrometer would be necessary. In addition to the simulation with measured spectra the calculation of the expected intensities matches the measured signal strength nearly perfect. The only exception is a constant offset which can have many reasons like a wear out of the lamp or sensors or a worse sensitivity of the sensors.

Comparing the NO and NO₂ results a clear signal increase is visible, when the absorption peaks of NO and the transmission peaks of the etalon overlap with a peak at around 22° deflection. This effect is not visible for NO₂ where a nearly constant signal strength is present. The signal increases for NO by a factor of 3.2 and for NO₂ only by a factor of 1.1. The explanation is a better overlap of the transmission lines for the 0° position and the 20° position of the etalon with the absorption spectra of the two gases (cf. figure 2.22). The transmission lines of the etalon do not overlap with the absorption peaks of NO therefore the signal (which is a difference signal of the two detectors) is low. For the NO₂ gas the difference caused by absorption between the two sensors is stronger. Shifting the etalon the signal stays nearly the same for NO₂ because of the flat absorption spectrum in this area. On the other hand the transmission peaks will overlap with the absorption peaks of NO at some point, therefore resulting in a stronger absorption on the measurement detector and an increase in signal.

Looking at the overlap of the transmission and absorption peaks (cf. figure 2.22) it is clearly visible that these two spectra do not perfect overlap. Stretching the etalon transmission lines to get a perfect overlap and doing the simulation of the etalon turning again leads to the signal plotted in figure 4.20. The signal increases at the same angle but the increase is higher. The ratio highest/lowest value for the simulation with the real etalon is 3.2 comparing to the value for an optimized etalon with 8.7. Therefore the separation between the NO contribution and the cross correlations would be more easy and more precise.

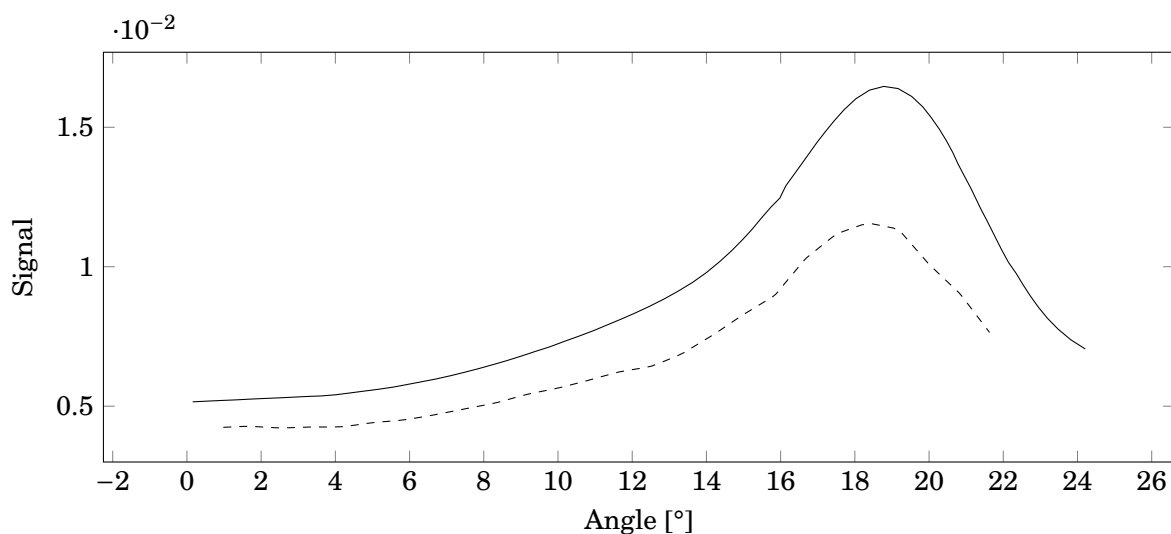


Figure 4.19: Simulation with the theoretical values from the manufacturers (solid) and simulation with measured data (dashed). The solid line fits the actual measurements quite well (cf. figure 4.18). The shift of the second simulation may result from the fact that the spectrometer was not intensity calibrated. The simulation with the spectrometer data was performed as described in section 4.3.4.3.

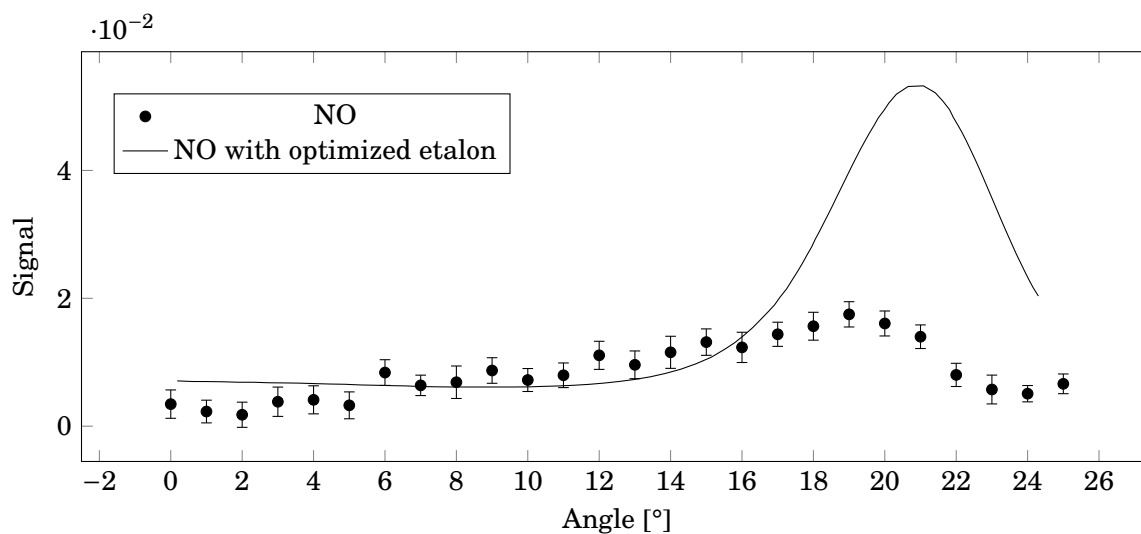


Figure 4.20: Signal from the real etalon (Number 5) and the simulated signal with an optimized etalon. The simulation with the optimized etalon was performed by Gerald Auböck at CTR. Highest/lowest value: 8.7

4.3.5 Discussion

Using only a rudimental breadboard setup a detection limit of around 50 ppm was found for a single shot measurement. When averaging over 1 second with a repetition rate of 177 Hz the

detection limit decreases to 2.3 ppm for NO. As the desired resolution of the final product is below 1 ppm this results confirms the possibilities using this method and the reached resolution is satisfying for the minimal setup. The cancellation of the cross correlations with the etalon method was demonstrated (c.f. figure 4.18).

Although these measurements with the basic bread board setup are promising there is a lot of room to increase the signal-to-noise ratio and enhance the selectivity. One step was the development of a custom made absorption cell which had in the first measurements a higher noise than the bread board setup but this was just the first test, so a noise as low as the bread board setup should be easily accomplished. Although the noise got higher the resolution increased as the absorption signal increased due to the advanced optical construction and the longer path-length. Due to the higher light intensity with the detection limit decreased from 50 ppm ($(0.3 \pm 0.1) \cdot 10^{-2}$) with the bread board setup to 10 ppm ($(0.6 \pm 0.2) \cdot 10^{-2}$) for a single shot. This increase of detection limit is due to the longer pathlength and the optimized optical elements. For a one second measurement with 177 Hz the detection limit is around 0.7 ppm.

Although the custom made cell increases the detection limit further improvements are possible, meaning a shorter measurement time or a higher resolution. The most promising performance improvement is at the moment the enhancement of the etalon in a way to match the NO absorption lines better. This is also probably the most difficult part to do it for a production series.

CONCLUSION AND COMPARISON

Fluorescence Due to the literature studies regarding the fluorescence a negative result was observed for the possibility to use this method for exhaust gas measurements in a mobile setup. The measurements were performed because a high selectivity was expected. In section 4.2.2 the signal for the background light intensity is shown. The minimization of this signal was one important task beforehand. This was done by choosing filters in the range of the excitation wavelengths (corresponds to the absorption wavelengths, c.f. figure 2.4) of NO and the fluorescence wavelengths (c.f. figure 2.13). Although these two wavelength areas are close together the two filters have as minimal overlap as possible (c.f. figure 3.6) for standard commercial available optics. For further reduction of the noise shielding around the photon counting tube and the two optical paths (c.f. section 3.2) was installed. Measurements with nitric oxide lead to a linear dependency of the fluorescence with the concentration (c.f. figure 4.3 and figure 4.4). This dependency was stated in the literature [26] until 7 ppm. At higher concentrations a self-quenching effect is observed. Due to the high uncertainty of our measurements (c.f. figure 4.3) this self-quenching effect can not be observed. Dilution of nitric oxide with synthetic air leads to a strong quenching of a factor of 10 due to oxygen which was investigated in the literature [16] before. Therefore a dilution with synthetic air to conquer the quenching of CO₂ like with N₂ is not possible (c.f. section 2.4.3, [21]). The NO fluorescence measurement with a NO₂ dilution leads to the same as for synthetic air (c.f. figure 4.9 and figure 4.10). This is due the fact that synthetic air is the carrier gas for NO₂. Fluorescence of NO₂ is not measured when using a filter with a transmission like in the setup (c.f. figure 4.8). Although the molecule is excited to higher states the fluorescence occurs at shorter wavelengths because of Kasha's rule (c.f. section 2.4.1). These quenching effects of oxygen and the expected quenching with carbon dioxide lead to the fact that fluorescence is not usable for mobile exhaust gas measurements. Nevertheless a stationary system with a dilution of

molecular nitrogen or a dilution in form of an expansion into a chamber with reduced pressure is possible. With this method measurements without cross correlations should be possible.

Absorption without etalon The first iteration of the setup for the absorption measurements was build with standard components and a special designed etalon (c.f. section 3.1.2). With the bread board setup the detection limit was around 50 ppm (c.f. section 4.3.3.1 and figure 4.14) with a signal of $(0.3 \pm 0.1) \cdot 10^{-2}$ for a single shot measurement. Switching to a custom made absorption cell with lenses in front of the sensors a reduction of the detection limit is performed. It is lowered to 10 ppm with a signal of $(0.6 \pm 0.2) \cdot 10^{-2}$ (c.f. section 4.3.3.2 and figure 4.15). Calculating the limit of detection for a one second measurement with a repetition rate of 177 Hz, considering a minimum signal-to-noise ratio of 3, leads to a value of 2.3 ppm for the bread board setup and to 0.7 ppm for the absorption cell.

The reduction is not a result of the reduced noise which was expected with the enclosed cell, furthermore it is because of the enhancement of the signal intensity itself due to the increased path length (+ 5 cm) and the enhanced optical parts.

Absorption with etalon As the selectivity for non-dispersive absorption measurements are strongly reduced in contrast to the fluorescence measurements the etalon approach had to be tested for cross correlations. Therefore the manual turning measurements were performed with NO and NO₂ as test gas flowing through the cell. These two measurements showed a clear increase in the signal for NO measurements, explained by the better overlap of the transmission peaks of the etalon and absorption peaks of NO (c.f. figure 2.4 and figure 2.23). Performing the same measurement with NO₂ leads to a nearly constant difference signal (c.f. figure 4.18) because of the relatively flat absorption cross section of NO₂ (c.f. figure 2.7). A simulation with the data from the manufacturer of the etalon and filter, the measured intensity spectrum of the flash lamp and the absorption cross section of NO and NO₂ (c.f. figure 2.4 and figure 2.7) leads to the same curves for these two gases as the measurement. As these results show that the cancellation of the cross correlations is working with the etalon approach it is possible to develop a measurement system using this method. Although further testing and improvements are required the proof of concept is done. Further improvements can be achieved by optimizing the etalon (c.f. section 4.3.4.3 and figure 4.20) and the reduction of noise with an encapsulation of the whole light path and enhanced sensors.

In conclusion to this thesis it is possible to say that the first investigated method, fluorescence, led to the expected results. Unfortunately these results confirm the expectation that this approach is not usable for mobile NO exhaust gas measurements, although this method would give a selectivity advantage. The second approach, absorption, was working better as expected, specially the filtering of the cross correlations in the area of NO absorption was satisfying and with further investigations an improvement to the desired detection limit of 1 ppm or lower should be possible.

6.1 Pulse energy

In this section the irradiance and the waveform for the pulse energy estimation in section 4.3.1.1 are given.

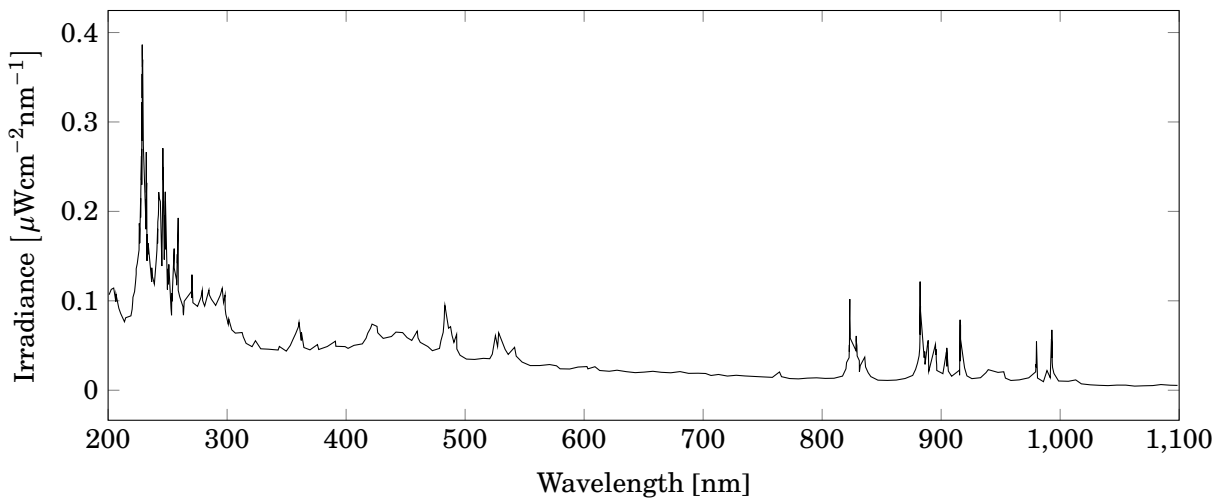


Figure 6.1: Spectral distribution of the Hamamatsu L9455-01 flash lamp (discharge capacitance $0.22 \mu\text{F}$) which behaves similar as the used L9455-13 lamp (discharge capacitance $0.047 \mu\text{F}$). Operations condition: discharge voltage 600 V, discharge capacitance $0.22 \mu\text{F}$, flash frequency 126 Hz, measurement distance: 50 cm [18]

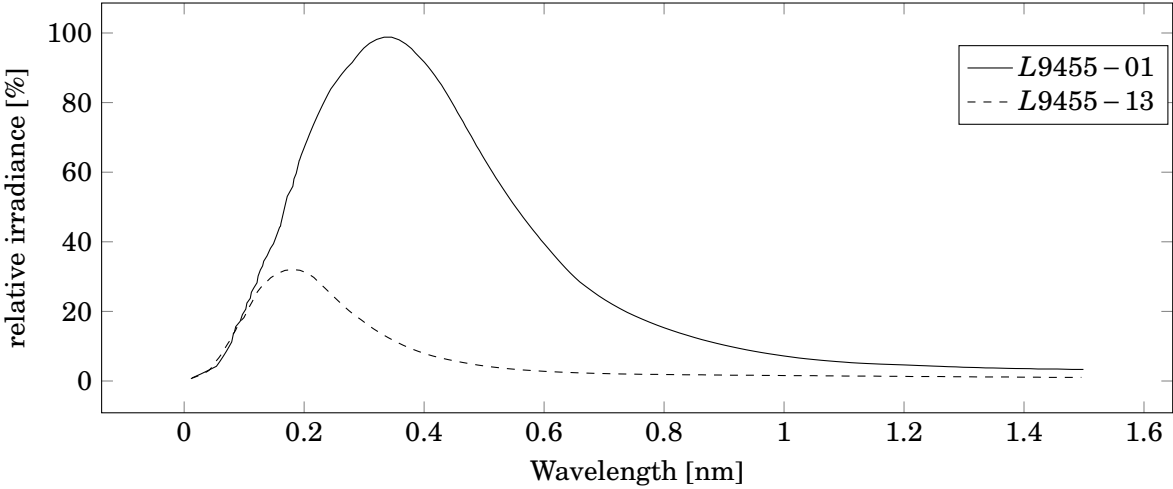


Figure 6.2: Waveform difference of the main discharge capacitance of the L9455-01 and the used L9455-13 flash lamp. With the ratio of those waveforms the puls energy is estimated. [18]

6.2 Used parts and devices

Table 6.1: Used parts in the setups, parts used in both setups are listed first.

Part	Manufacturer	Number	Specification
Flashlamp	Hamamatsu	L9455-13	
Coupling	Thorlabs	various	
Optical Rail	Thorlabs	various	
Dovetail Rail Carriers	Thorlabs	various	
Optical Posts	Thorlabs	various	
Post Holders	Thorlabs	various	
Lens	Thorlabs	LA4936	
Filter	LOT-Quantum Design GmbH	214FS22	Peak 214 ± 3 nm, FWHM 22 ± 4 nm
Enclosure	Thorlabs/Self-made		
Etalon	LayerTec	custom	
Lens	Thorlabs	LA4130	
Breadboard	Thorlabs	various	
Mass Flow Controller	Vögtlin		
Fibre		various	
Absorption setup			
Lens	Thorlabs	LA4130	
Flowcell	Starna	34GL14s	
V-Clamp	Thorlabs		
Mirror	Thorlabs	PF10-03-F01	
3-Axis Stage			
Detectorboard	self-made		
High-Precision Rotation Mount	Thorlabs	PR01/M	
Fluorescence setup			
Filter	LOT-Quantum Design GmbH	265FS25	Peak 265 ± 3 nm, FWHM 25 ± 5 nm
Flowcell	Starna	46-F/Q/10	
Cellholder	self-made		
Mirror	Thorlabs	CM254-019-F01	
Lens	Thorlabs	LA4052	
Photomultiplier	Hamamatsu	R943-02	
Beamtrap			

BIBLIOGRAPHY

- [1] L. Bergmann, H. Niedrig, and H.J. Eichler.
Optik: Wellen- und Teilchenoptik.
Bergmann. de Gruyter, 2004.
- [2] Wolfgang G. Bessler, C Schulz, and Jay B Jeffries.
Strategies for quantitative NO-concentration and temperature measurements by NO LIF in
high pressure flames.
Conference Paper, 1990.
- [3] A B Callear and I W M Smith.
Fluorescence of Nitric Oxide, Part 1.
Trans. Faraday Soc., 59:1720–1734, 1963.
- [4] A B Callear and I W M Smith.
Fluorescence of Nitric Oxide, Part 2.
Trans. Faraday Soc., 59:1735–1747, 1963.
- [5] V. M. Donnelly, D. G. Keil, and F. Kaufman.
Fluorescence lifetime studies of NO₂. III. Mechanism of fluorescence quenching.
The Journal of Chemical Physics, 71(2):659–673, 1979.
- [6] Institut für Experimentalphysik der Technischen Unverisität Graz.
Experimentelle Methoden der Spektroskopie, Quantenoptik und Quantenmesstechnik.
Institut für Experimentalphysik der Technischen Unverisität Graz, 2013.
- [7] Harald Gaulhofer.
Ottomotor und Dieselmotor im Vergleich.
Diplomarbeit, Hochschule Mittweida, 2015.
- [8] Gary D. Greenblatt and A. R. Ravishankara.
Collisional quenching of NO (A, v' =0) by various gases.
Chemical Physics Letters, 136(6):501–505, 1987.

- [9] N V Heeb, A M Forss, and C Bach.
Fast and quantitative measurement of benzene, toluene and C₂-benzenes in automotive exhaust during transient engine operation with and without catalytic exhaust gas treatment.
Atmospheric Environment, 33(2):205–215, 1999.
- [10] Jablonski-Diagramm.
https://de.wikipedia.org/wiki/Jablonski-Schema#/media/File:Jablonski_Diagramm_Deutsch.png.
05.12.2016.
- [11] Prof. Jose-Luis Jimenez.
Lecture 7: Photochemistry of important atmospheric species.
http://cires1.colorado.edu/jimenez/AtmChem/CHEM-5151_S05_L7.pdf.
3.1.2017.
- [12] H. Keller-Rudek, G. K. Moortgat, R. Sander, and R. Sørensen.
The MPI-Mainz UV/VIS Spectral Atlas of Gaseous Molecules of Atmospheric Interest.
Earth System Science Data, 5(2):365–373, 2013.
- [13] U. Kilian and C. Weber.
Lexikon der Physik - Sonderausgabe: Buch-Gesamtausgabe, 5 Bände + 1 Registerband.
Spektrum Akademischer Verlag, 2003.
- [14] Wieland Koban, Jon D. Koch, Ronald K. Hanson, and Christof Schulz.
Absorption and fluorescence of toluene vapor at elevated temperatures.
Physical Chemistry Chemical Physics, 6(11):2940, 2004.
- [15] Joseph R. Lakowicz.
Quenching of Fluorescence, pages 277–330.
Springer US, Boston, MA, 2006.
- [16] L A Melton and W Klemperer.
Quenching OF NO A₂X+ BY O₂X³Σ.
Planetary and Space Science, 20(2):157–160, 1972.
- [17] H D Mettee.
Fluorescence and phosphorescence of SO₂ vapor.
Journal of Chemical Physics, 49(4):1784–1793, 1968.

- [18] Datasheet: 5 W Xenon Flash Lamp Modules.
http://www.hamamatsu.com/resources/pdf/etd/5W_Xe-F_TLSZ1006E.pdf.
28.04.2017.
- [19] G. H. Myers, D. M. Silver, and F. Kaufman.
Quenching of NO₂ Fluorescence.
The Journal of Chemical Physics, 44(2):718–723, 1966.
- [20] Illustration of Kasha's rule in spectroscopy.
https://en.wikipedia.org/wiki/Kasha's_rule#/media/File:Kasha-s-rule.png.
28.02.2017.
- [21] Hideo. Okabe.
Fluorescence quenching of sulfur dioxide by source emission gases.
Analytical Chemistry, 48(11):1487–1489, 1976.
- [22] Robert Opitz.
https://de.wikipedia.org/wiki/Stern-Volmer-Gleichung#/media/File:Stern-Volmer-Plot_2.jpg.
28.02.2017.
- [23] M. Orain, P. Baranger, B. Rossow, and F. Grisch.
Fluorescence spectroscopy of naphthalene at high temperatures and pressures: Implications for fuel-concentration measurements.
Applied Physics B: Lasers and Optics, 102(1):163–172, 2011.
- [24] Josué Reboux, Daniel Puechberty, and Frédéric Dionnet.
A new approach of planar laser induced fluorescence applied to fuel/air ratio measurement in the compression stroke of an optical si engine.
Technical report, SAE Technical Paper, 1994.
- [25] Wolfgang Schneider, Geert K. Moortgat, Geoffrey S. Tyndall, and John P. Burrows.
Absorption cross-sections of NO₂ in the UV and visible region (200 - 700 nm) at 298 K.
Journal of Photochemistry and Photobiology A: Chemistry, 40(2):195 – 217, 1987.
- [26] Frederick P. Schwarz and Hideo. Okabe.
Fluorescence detection of nitric oxide in nitrogen.
Analytical Chemistry, 47(4):703–707, 1975.
- [27] Masako Suto, Xiuyan Wang, Jun Shan, and L. C. Lee.
Quantitative photoabsorption and fluorescence spectroscopy of benzene, naphthalene, and some derivatives at 106-295 nm.
Journal of Quantitative Spectroscopy and Radiative Transfer, 48(1):79–89, 1992.

- [28] Gregory J Thompson, Daniel K Carder, Marc C Besch, Arvind Thiruvengadam, and Hemanth K Kappanna.
In-Use Emissions Testing of Light-Duty Diesel Vehicles in the United States.
Technical Report, (202), 2014.
- [29] Volkswagen AG.
Motor Vehicle Exhaust Emissions : Composition, Emission, Standards, etc.
Self Study Program VW Audi, 1:2–22, 2012.
- [30] Christian Walz.
NO_x-Minderung nach dem SCR-Verfahren: Untersuchungen zum Einfluß des NO₂-Anteils.
2000.
- [31] K. Watanabe, Edward C. Y. Inn, and Murray Zelikoff.
Absorption Coefficients of Nitrogen Oxide in the Vacuum Ultraviolet.
The Journal of Chemical Physics, 21(6):1026–1030, 1953.
- [32] Gerhard Wiegleb.
Gasmestechnik in Theorie und Praxis - Messgeräte, Sensoren, Anwendungen.
Springer Vieweg, 2016.
- [33] Barbara Zielinska, John Sagebiel, Jacob D Mcdonald, Kevin Whitney, and Douglas R Lawson.
Emission Rates and Comparative Chemical Composition from Selected In-Use Diesel and Gasoline-Fueled Vehicles.
Journal of the Air & Waste Management Association, 54(9):1096–2247, 2004.